Development of Portable Surface-Enhanced Raman Spectroscopy Nanosensors for Ultrasensitive Characterization of Drugs in Human Biofluids

Department of Chemistry and Chemical Biology
Indiana University-Purdue University Indianapolis

Trustees of Indiana University

Rajesh Sardar, Ph.D., Professor

Award number: NIJ 2018-75-CX-0034

Project Period: 1 January 2019 – 31 December 2022

Award Amount: $445,244.00

List of Abbreviation

SERS: Surface-enhanced Raman scattering (SERS)
LC-MS: Liquid chromatography-mass spectrometry
GC-MS: Gas chromatography-mass spectrometry
ELISA: Enzyme-linked immunosorbent assay
SWGTOX: Scientific Working Group for Forensic Toxicology
Au TNP: Gold triangular nanoprism
LSPR: Localized surface plasmon resonance
EM: Electromagnetic
EF: Enhancement factor
DDA: Discrete-dipole approximation
NP: Nanoparticle
AFM: Atomic force microscopy
TEM: Transmission electron microscopy
SEM: Scanning electron microscopy
TEA: Triethylamine
PMHS: Polymethylhydrosiloxane
PEG: Polyethylene glycol
APTES: Aminopropyltriethoxy silane
PHTMS: Phenyltriethoxysilane
OCTMS: Octyltrimethoxysilane
LOD: Limit of detection
TDDFT: Time-dependent density functional theory
DOA: Drug-of-abuse
ED: Emergency department
AUC: Area under the curve
ROC: Receiving operating characteristic
PCA: Principal components analysis
DA: Discriminant Analysis
PCR: Principal component regression
CCR: Constant contact radius
CCA: Constant contact angle
AEF: Analytical enhancement factor
Au NR: Gold nanorod
PSI: Paper spray ionization

➢ PROJECT SUMMARY

1. Goals of the Project: The overarching goal of this project is to fabricate entirely new, ultrasensitive, and flexible surface-enhanced Raman scattering (SERS)-based nanosensors that can be used for toxicological drug analysis directly from biological fluids.

2. Objectives of the Project. Currently, there is no way to assay (detection and quantification) <10 ppb (10 ng/mL) drugs in human biofluids without extensive sample processing either at bedside or roadside. The simple, fast and efficient assay of drugs and the identification of exposed individuals will greatly benefit law enforcement agencies and various toxicologists. Ultrasensitive, reliable, and rapid analyses will assist immediate forensic toxicology applications by law enforcement and promote aggressive efforts to eradicate drugs from communities. The objectives of this projects are:

Objective 1: Construct unique SERS nanosensors for ultrasensitive toxicology analysis (detection, identification, and quantification) of drugs in biofluids (e.g., plasma, whole blood, saliva, urine, and sweat).

Objective 2: Avoid fouling and matrix effects while identifying drugs at low (e.g., pg/mL) concentrations in blood plasma and apply chemometric analysis to discriminate drugs with highly similar SERS spectra and to resolve the SERS spectra with known metabolites and in biological matrices.

3. Research Questions: Toxicological analysis of unknown drugs is extremely challenging using the current analytical techniques such as LC/MS, GC/MS, and ELISA due to low sensitivity, interference of the biological matrix, and/or the lack of available antibodies.[1-7] The half-life of opiates is a few minutes to hours as these drugs decompose very fast in the metabolic system. Therefore, the concentration of intact drug is expected to be exceedingly low, and thus many analytical methods, as mentioned above, rely on identifying metabolites instead of the actual drug. In this context, many metabolites have similar m/z values and chance of a false response is very high. These current shortcomings have resulted in an unmet need for the development of a widely applicable, label-free, highly selective and quantitative analytical technique capable of assaying (detection and quantification) exceedingly low quantities of highly potent drugs in human biofluids.

The development of an instrumental method/sensor for forensic toxicology applications must address several key prerequisites of instrument/sensor ability as recommended by the Scientific Working Group for Forensic Toxicology (SWGTOX)[8] : Sensitivity (quantification): Is the instrument responsive to low analyte concentration? It is commonly defined as the slope of the calibration curve for an analyte. Selectivity (detection): Is there an ability to respond to an analyte despite the presence of interferents (e.g., biological matrix)? Specificity (identification): Is there an ability to unambiguously identify the analyte? Reproducibility (reliability): Is there an ability to repeatedly analyze samples (identify analytes) with high selectivity and specificity?

In forensic toxicology, these factors are interrelated as many evidence types contain trace levels of drugs (e.g., drugs in biofluids). Ultra-low levels (~pg/mL) of detection are also crucial for forensic applications where the concentration of drugs is exceedingly low due to rapid metabolic

decomposition. Further, an analytical technique with high selectivity is extremely important as most toxicological samples contain biological matrix that can compromise the accuracy of the measurement and may lead to false negative results. Specificity is required for forensic methods that are offered as probative evidence. Importantly, reproducibility of the analysis, including sensor stability, is a key factor because this demonstrates the reliability of a technique. The proposed method will satisfy all of the SWGTOX validation criteria to fill the gap of in-the-field rapid sample analysis for court-admissible data for criminal justice purposes.

A critical question is how do the chemistry, forensic, healthcare, and law enforcement communities overcome the drawbacks of existing analytical methods in order to achieve highly reliable quantitative toxicological sample analysis in the field non-invasively that will yield court admissible data? As illustrated in Figure 1, this project has undertaken the tasks to address the following questions.

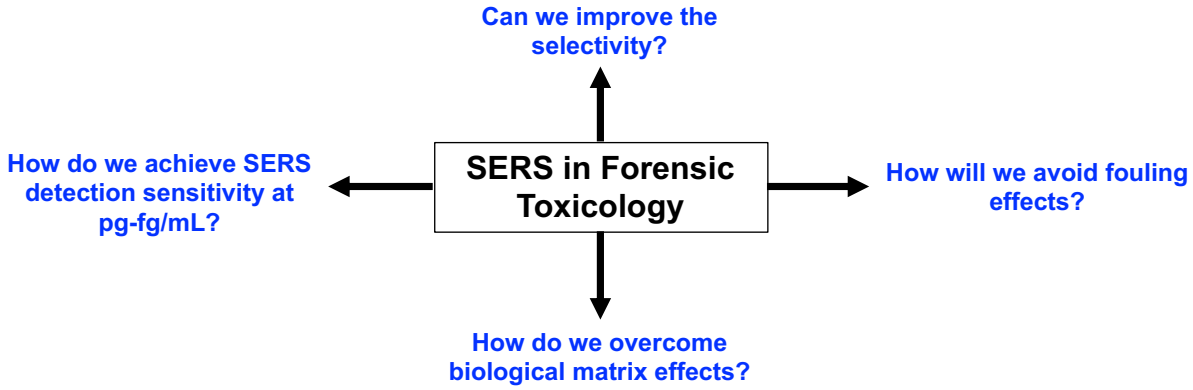

Figure 1. The overall summary of the project for the construction of ultrasensitive and highly selective SERS-based nanosensors, which can function in human biofluids.

4. Summary of Project Design and Methods: The novelty of this proposal stems from the choice of gold triangular nanoprisms (Au TNPs) as the SERS substrate for the fabrication of self-assembled nanosensors, along with appropriately selected surface ligand chemistry. Au TNPs and their surface chemistry provide the following unique advantages:

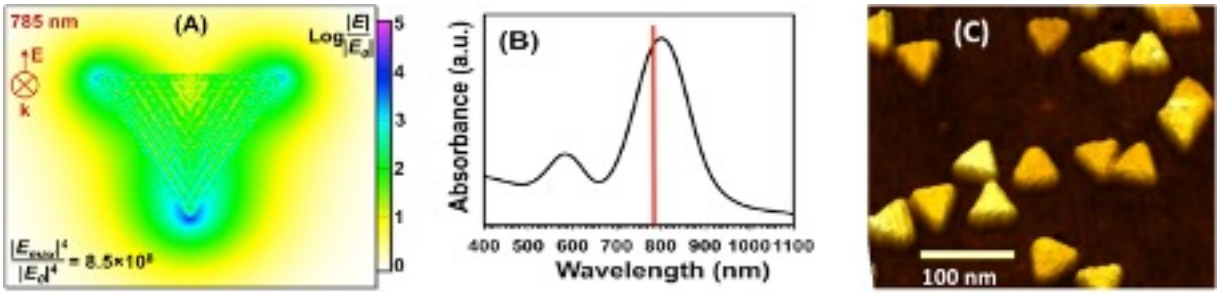

Figure 2. *(A) Local field intensity enhancement at 785 nm excitation for an Au TNP. The polarization direction is vertical. The plot is in logarithmic scale, where white is the lowest and magenta is the highest (B) UV-vis spectrum of Au TNPs on 3M adhesive tape. Au TNPs display their strongest LSPR peak at 800 nm. The peak at 570 nm represents an LSPR peak associated with the thickness of Au TNP. The red line represents the laser excitation wavelength (785 nm). (C) AFM image of the Au TNPs used for our nanosensor fabrication.*

(1) As illustrated in **Figure 2**, discrete-dipole approximation simulations (DDA) of our chemically synthesized Au TNPs with average edge-length of ~42 nm and ~8 nm in thickness show strong electromagnetic (EM)-field enhancement at the sharp tips and edges. Recent publications [9-11] from the Sardar group demonstrate that Au TNPs form an attractive and ultrasensitive SERS substrate for nanotechnology-based sensing. The efficiency of SERS is characterized by the enhancement factor (EF) for a given SERS substrate. EF is defined by Raman signal amplification over normal conditions (i.e., without using metallic NPs). Thus, the higher the SERS EF, the higher the sensitivity. SERS EFs of ~10-10^3 can be achieved with standard NPs, with some values in the range of ~10^5-10^6.

(2) The localized surface plasmon resonance (LSPR) peak position of metal NPs and the wavelength of the incident light source (i.e., the laser) control the hot spot intensity. An ideal NP for SERS application would be one whose LSPR peak is longer than but very close to the wavelength of the laser source. For many forensic applications, laser excitation with low energy photons (e.g., 785 nm) avoids sample decomposition. The LSPR peak of our Au TNPs appears at ~800 nm (**Figure 2**) making them ideal SERS substrates as compared to Ag NPs, which display an LSPR peak <600 nm and have been previously used for forensic SERS applications [12-16].

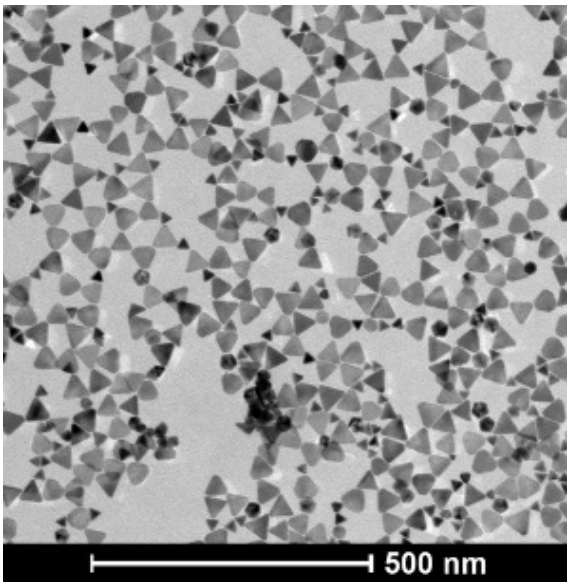

Figure 3. A representative transmission electron microscopy (TEM) image of Au TNPs. Adapted from Sardar et al. Analyst 2020.

(3) An atomic force microscopy (AFM) (**Figure 2**) and the transmission electron microscopy images (**Figure 3**) of Au TNPs show an atomically flat surface with triangular shape. Thus, their geometry is appeared to be prismatic in the nanometer dimension, so we refer them as **"triangular nanoprisms"**. Therefore, analytes can adsorb with a much more uniform density as compared to spherical-shaped metal NPs. The Au TNP surface also provides additional advantages in terms of transferring drugs from solid surfaces such as human skin.

(4) The stability of the SERS substrate is critical. Au is very stable under ambient conditions and in solution, photo-bleaching under laser excitation in SERS analysis is negligible compared to Ag which decomposes much faster under similar conditions. Therefore, our Au TNP-based nanosensor not only provides reproducible data but is also ideal for SERS measurements in various human biofluids. Another important criterion for fabrication of SERS nanosensors is that the NPs should be supported by a microscopically flat surface (e.g., a glass slide and a silicon substrate). We also selected adhesive tape because its "stickiness" creates a stronger hold on the Au TNPs and analyte molecules can be extracted from the solid surface more efficiently. Further, the flexibility of the adhesive tape should allow our nanosensor to closely touch a complex

surface without destroying it, as demonstrated for SERS-based pesticides detection on fruits [17]. Finally, adhesive tape is stable when exposed to many biofluids (e.g., plasma, whole blood, urine, sweat, and saliva), the same media that most toxicological analysis is conducted. Therefore, a drug sample can be directly drop-casted onto our SERS nanosensor for analysis without any extraction and purification. Most importantly, the non-toxic nature of adhesive tape is expected to enhance our nanosensor stability, which is the number-one problem with existing SERS sensors. Therefore, we expect unprecedented reproducibility in measurements with bench-top and handheld Raman instruments. Also, as discussed below we will conduct in-depth investigation on temperature dependent stability and reproducibility of the SERS nanosensors.

(5) The forensic toxicology laboratories nationwide have accepted the matrix effects as an essential part in the validation of any LC-MS (/MS)-based methods. Also, it has been suggested for the LC-MS (/MS) method that the matrix effects can be reduced either by diluting samples or injecting a small amount of samples[18,19]. However, this process is only applicable when the sensitivity of the assay is very high, in which the LC-MS (/MS) technique would be clearly lacking for use in such an approach because of its low sensitivity. To address the four questions that are listed in Figure 1, we investigated two separate but interconnected chemical approaches for the fabrication of ultrasensitive, SERS-based nanosensors, which can analyze potent drugs in diluted human plasma samples. We detected drugs in diluted plasma to reduce the matrix effect.

(6) In the development of SERS nanosensors utilizing plasmonic nanoparticles for the analyte detection, two important factors need serious consideration: (1) Generation of a large number of EM hot spots. It is reported that a near-field plasmonic coupling between metallic nanoparticles with sharp tips such as nanostars and TNPs provides significantly higher SERS enhancements compared to spherical nanoparticles and nanorods.[20-24] Furthermore, SERS enhancement drastically decreases as analyte molecules move too far from the SERS substrates.[25,26] (2) Avoid "fouling" which is characterized as competing adsorption of analyte molecules reaching to the electromagnetic hot spots.[27] The most common approach in SERS-based chemical sensing is to drop-cast the analyte solution onto the SERS nanosensors. This non-specific adsorption of analytes onto a SERS-active surface only works for pure analytes. Successful implementation of SERS to chemical diagnostic and forensic toxicology requires detection of analytes in blood plasma, which contains plasma proteins. The proteins and analyte compete to reach electromagnetic hot spots via diffusion which results in an increase in background noise that eventually reduces the sensitivity and specificity of the assay.

The entire project has been studied in two parts: (1) Investigating how to optimize the EM hot-spots in the Au TNP assembly for an ultrasensitive drug detection using nanoplasmonic superlattice SERS substrates; and (2) Performing chemical modification of SERS substrates (**"plasmonic patches")** to avoid fouling effects for potent drug analysis in human blood plasma. Therefore, the first component is described in **Section 4.1 and 5.1**, and the second component is outlined in **Section 4.2 and 5.2**. Both the parts will be using the identical Au TNP synthesis as described in Section 4.1. Thus, it will not be repeated in Section 4.2.

4.1. Experimental Methods.

Synthesis of gold triangular nanoprisms (Au TNPs). Au TNPs were synthesized according to our published methods.[28,29] Briefly, $Et_3PAu(I)Cl$ (0.010 g) was dissolved in 20 mL of N_2-purged CH_3CN and stirred for 5 min at room temperature followed by the addition of 0.019 mL of TEA. The temperature of the reaction mixture was then gradually increased to 40 ℃. At this desirable temperature, 0.3 mL of PMHS was added. The reaction was allowed to proceed at this temperature and during this time the solution changed from colorless to pink, blue, and then deep purple. The formation of Au TNPs and their corresponding edge-lengths were characterized by UV-Vis absorption spectroscopy by monitoring the dipole peak position (λ_{LSPR}) of Au TNPs. Once the λ_{LSPR} of Au TNPs in CH_3CN reached 800 nm (**Figure 2B**), the reaction mixture was removed from heat, centrifuged at 5000 rpm for 5 min, and the solution was used for the preparation of nanoplasmonic superlattice substrates. Previously, we determined that the average edge length of Au TNPs, which display an λ_{LSPR} at ~800 nm in CH_3CN, is 42 nm.[29,30]

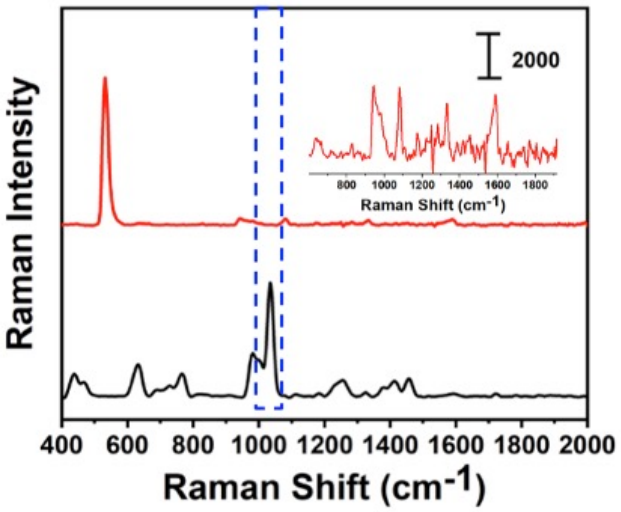

Figure 4. (Bottom) The SERS spectrum of TEA-passivated Au TNPs. The Raman stretch at 1035 cm^{-1} is assigned to the C-N stretch of TEA used for the synthesis of the Au TNPs. **(Top)** The SERS spectrum collected after 24 h ligand exchange with 1.0 mM of PEG60-SH. The complete disappearance of C-N stretch (1035 cm^{-1}, blue dotted box) confirms the successful replacement of TEA, and the formation of PEG60-S-functionalized Au TNPs. The inset shows an expanded version of the top spectrum showing peaks at 645, 944, 1083, 1100 and 1177, and 1334 cm^{-1} for aliphatic C-S stretch, C-H bending, COC symmetric stretch, and CH_2 stretch, respectively.[31] The scale bar is for the overall spectra and not for the inset. Adapted from Sardar et al. Analyst 2020.

Preparation of nanoplasmonic superlattice substrates. Nanoplasmonic superlattice substrates for the SERS-based drug analysis were prepared as follows: (1) Synthesized Au TNPs were attached onto aminopropyltriethoxy silane (APTES)-functionalized glass coverslips by incubating for 1 h. The Au TNP-bound coverslips were washed thoroughly with acetonitrile to remove loosely adsorbed organic compounds (e.g., PMHS and TEA) and dried under N_2 flow that display λ_{LSPR} extinction peak at 775 nm in air. (2) Coverslips containing Au TNPs were incubated in a 1.0 mM polyethylene glycol thiol (PEG60-SH) solution for overnight. This resulted in complete ligand exchange, as confirmed by SERS measurements (**Figure 4**). The PEG60-S-functionalized Au TNPs were placed in a glass container containing 2 mL ethanol and were sonicated for 5 min in an ice-cold water bath. During the sonication, the PEG60-S-functionalized Au TNPs were lifted off the solid support into solution due to weak Au-NH_2 interactions. (3) The ethanolic solution containing PEG60-S-functionalized Au TNPs was centrifuged for 1 min at 13,000 rpm and resulted in a blue solid, which was collected, re-dissolved in 1 mL ethanol and centrifuged again.

The process was carried out at least 5 times to remove excess/loosely bound PEG60-SH. After the final wash, PEG60-S-functionalized Au TNPs were dissolved in 100 µL of nanopure water and sonicated for 5 min to prepare a homogeneous solution. (4) 25 µL of the blue solution containing PEG60-S-functionalized Au TNPs was drop-casted onto an APTES-/PHTMS-/OCTMS-modified silicon wafer and the solvent was allowed to evaporate under room temperature and 60 ± 5% humidity.

Time-dependent density functional theory (TDDFT) calculations. TDDFT calculations were performed to determine Raman vibrational frequencies of various drug molecules. Calculations involved geometry optimization and calculations using Gaussian16 with the B3LYP hybrid exchange correlation functional and 6-311+G** basis set[32] for free drug molecules and drug molecules attached to the glycol moiety. Calculations were also performed for drug molecules attaching to a gold (Au) atom using the BP86 exchange-correlation functional and the LanL2DZ effective core potential basis set.[33] Gaussview 6.0.16 was used to visualize the optimized geometry and assign the vibrational modes.[34]

Analytical measurements. SERS measurements were conducted using a Foster-FORAM 785 HP Raman system with a 785 nm diode laser excitation source with 20 mW of power and 5-µm spot size. Automatic baseline correction was performed using OMNIC software before acquired spectra were plotted. A Varian Cary 50 Scan UV-visible spectrophotometer was used to collect absorption and extinction spectra in the range of 300-1100 nm. For the absorption spectra of Au TNP solutions, 0.3 mL of reaction mixture was diluted to a final volume of 2.0 mL with acetonitrile in a 1 cm quartz cuvette. Acetonitrile was used as a background in each run before collecting absorbance spectra. Extinction spectra of PEG60-S-functionalized Au TNPs as a nanoplasmonic superlattice substrate were collected using a Perkin Elmer Lambda 19 UV-Vis-NIR spectrometer. APTES-/PHTMS-/OCTMS-functionalized glass coverslips were used as a background. Nanoplasmonic superlattice substrates were imaged using a JEOL 7800F SEM instrument. TEM analysis was conducted using a Tecnai-12 instrument at 100 kV operating voltage. Colloidal acetonitrile solution of Au TNPs was drop-casted onto a Cu-carbon grid and the solvent was allowed to dry at room temperature before imaging. We used Ramé-Hart Contact Angle Goniometer to measure the contact angles.

4.2. Experimental Methods

For this part of the project, we used an identical Au TNP synthesis, PEG60-thiol surface modification, and same analytical characterizations as described above, thus not repeating the same information again. Several other new information pertinent to the work are listed below.

Binary mixture analysis. For binary mixture analysis, different weight percentages of fentanyl in heroin ranging from 0-100% were made (mass/mass percent composition). A total of 6 µL (2 x 3 µL) was dropcasted on the plasmonic patch and analyzed using SERS. The ratios of peak intensity for fentanyl in heroin were calculated using Eq 1:

$$R = \frac{(I_A - I_B)}{(I_A + I_B)} \qquad (1)$$

Where I is the peak intensity after baseline correction and R is the resulting ratio. Here, A represents the first drug molecule (fentanyl) and B represents the second drug molecule (heroin). All SERS spectra were plotted, and each peak intensity was determined using Origin software.

Peak intensity was determined by taking the average of three measurements. The calibration curve was obtained by plotting calculated peak intensity ratio vs percentage of fentanyl in heroin. Fitting was performed in Origin using a Langmuir isotherm with Eq 2:

$$\theta = \frac{qbx}{(1+bx)} \qquad (2)$$

Where, θ is the calculated peak intensity ratio, x is the percent fentanyl in heroin, and qb is the initial slope of the curve where q is the maximum ratio threshold and b is considered to be the affinity coefficient of fentanyl to the surface.

Statistical analysis. Unpaired t-test and area under the curve (AUC) of the receiver operating characteristic (ROC) graphs were plotted using GraphPad Prism. Unpaired t-test used the following p value style: 0.1234 (ns), 0.0332 (*), 0.0021 (**), 0.0002 (***), <0.0001 (****), and was performed at the 95% confidence interval. AUC of ROC was also performed at the 95% confidence interval.

Chemometric analysis. All multivariate statistical calculations were performed using XLSTAT (Version 2020.4.1, Addinsoft, New York). SERS spectra ranging from 0 – 100% fentanyl were normalized to unit vector length by dividing each value by the square root of the sum of squares of all values in the spectrum. Principal Component Analysis (PCA), Discriminant Analysis (DA), and Principal Component Regression (PCR) were then performed.

SERS-based drug analysis using different substrates. To develop fentanyl calibration curves, various concentrations ranging from 1.0 mM to 1.0 nM of fentanyl were prepared in 10% human plasma in RNA-free water. A total of 6 µL (2 µL X 3) of the fentanyl solutions were drop-casted onto SERS based plasmonic patches and allowed to dry overnight. For other drug analysis (cocaine, JWH-018, 4-ANPP, and heroin), 1.0 mM and 1.0 nM were prepared in 10% human plasma in RNA's free water and the resulting solution was drop-casted onto plasmonic patches similarly to the process described for fentanyl analysis. SERS spectra for each drug/ concentration were collected and the average SERS intensity value was determined from a minimum of six measurements. Identical dilution factor and protocol were followed for patient sample analysis using plasmonic patch as SERS substrates.

Preparation of plasmonic patches and drug detection. Au TNPs with ~42 nm edge lengths were synthesized according to our published procedure (see Supporting Information for additional details).[29,30] Au TNPs in acetonitrile were immobilized onto an APTES-functionalized glass substrate through incubation to form a self-assembled layer of TNPs. The Au TNP-bound coverslips were then incubated in a 1.0 mM PEG_{60}-SH solution for overnight for the ligand exchange. Next, 3M adhesive tape was placed on the PEG-S-functionalized Au TNP-containing glass substrate, pressed gently with the thumb, and removed at a 90^0 angle. This procedure resulted in successful transfer of the self-assembled Au TNPs from the glass to the flexible adhesive substrate, producing the plasmonic patch (Figure 1C). Drug detection and quantification were performed by directly drop-casting on to the SERS plasmonic patch, followed by slow evaporation of solvent at room temperature.

Limit of detection (LOD) and SERS EF calculations. LOD Calculations: Calibration curves were developed by plotting average peak intensity vs. logarithm scale of drug concentration in order to investigate non-specific adsorption at a lower concentration range. The calibration curve equations were determined through linear regression on Excel. The limit of detection (LOD) was determined by using a Z value of the blank (Z= mean + 3σ, σ = standard deviation), which was obtained using two different spots in three independently fabricated sensors (a total of six SERS measurements) and plugging the Z value into the "Y" in the calibration curve equation and obtaining the LOD concentration ("X"). **SERS EF calculations:** We followed a previously published method to calculate the enhancement factor of our plasmonic patches at the fentanyl 1384 cm^{-1} Raman peak, using a literature procedure.[35] N_{SERS} was calculated by using a laser spot diameter of 5 μM and a fentanyl molecule footprint of 0.76 nm^2.[35]

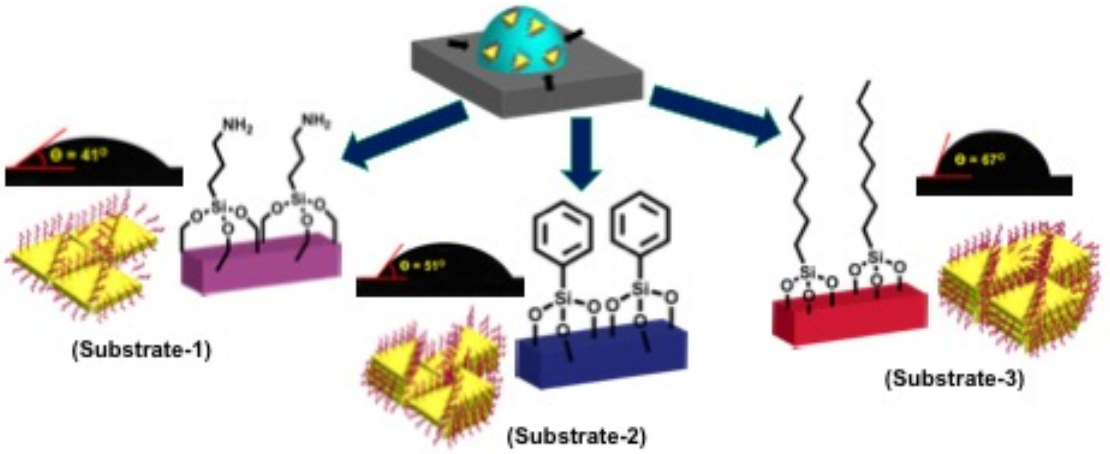

Figure 5. Schematic illustration of the droplet evaporation-based preparation of the nanoplasmonic superlattice substrate for the SERS-based drug analysis. The solid support dependent contact angle images of an aqueous solution of PEG60-S-functionalized Au TNPs are also shown. Adapted from Sardar et al. Analyst 2020.

5. Summary of Results:

5.1. Superlattice SERS Substrates for Ultrasensitive Drug Assay in Human Plasma. The work presented herein is based on the hypothesis that the hydrophilic, PEG60-S-coated, colloidal Au TNPs spontaneously self-assembled onto hydrophobic surfaces through droplet evaporation method to form 3D nanoplasmonic superlattices of strongly coupled TNPS producing a larger number of electromagnetic *"hot spots"* that contribute to outstanding SERS enhancement, allowing for the detection of potent drugs in ppq concentrations.[36,37] **Figure 5** illustrates the preparation of nanoplasmonic superlattices onto different silane-functionalized silicon supports. We selected Au TNPs to prepare the 3D superlattice SERS substrate because of the following optoelectronic and structural properties: (1) Sharp tips and edges produce strong electromagnetic field (EM) enhancement that, in turn, produces large SERS enhancement factors.[21] (2) PEG60-S-coated Au TNPs display an λ_{LSPR} extinction peak at 835 nm in air, which is higher in wavelength than the 785 nm diode laser excitation source used. Therefore, we expect a maximum SERS enhancement factor due to the higher energy incident laser excitation photons in comparison to the λ_{LSPR} of Au TNPs.[21,38] Moreover, a 785 nm laser source should avoid drug decomposition,

particularly in real world samples. (3) High stability of the Au-S bond due to soft-soft covalent interaction[30] is expected to produce stable PEG60-S-functionalized Au TNPs for the preparation of highly reproducible SERS substrates. (4) Flat surfaces of Au TNPs[39,40] should promote homogeneous PEG60-SH functionalization that would enable an excellent self-assembly process to form the desired 3D nanoplasmonic superlattice. Furthermore, PEGs reduce non-specific adsorption of endogenous biomolecules that are commonly present in human plasma.[41] Therefore, PEG60-S-functionalized Au TNPs should enhance selectivity in drug analysis. Finally, N-containing drugs (e.g., cocaine, fentanyl, and JWH-018) are expected to form hydrogen bonding with PEGs in an aqueous medium; this would allow ultrasensitive drug analysis in human biofluids.

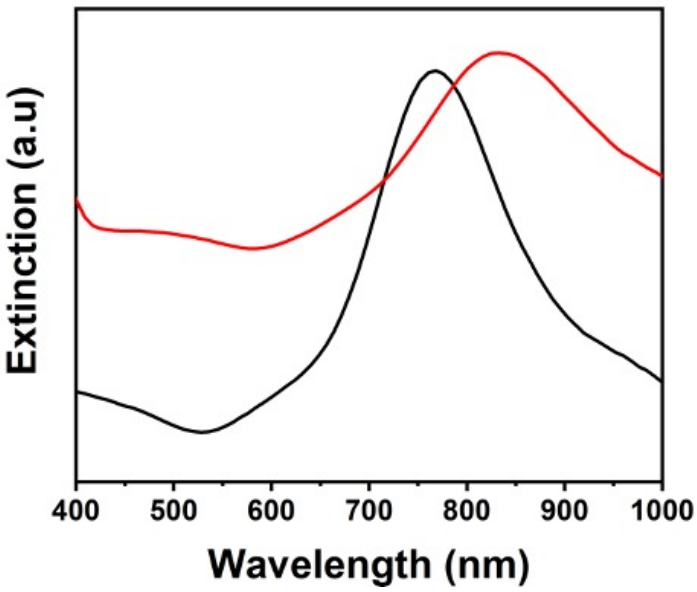

Figure 6. A UV-vis extinction spectrum of TEA-passivated Au TNPs attached onto an APTES-modified glass support. The LSPR dipole peak is at 775 nm (black). Ligand exchange with 1.0 mM PEG60-SH produces a red shift in the LSPR dipole peak and appears at 835 nm. All extinction spectra were collected in air. Adapted from Sardar et al. Analyst 2020.

5.1.1. Programmable-Prepared and Characterized Nanoplasmonic Superlattice Substrates. PEG60-S-coated Au TNPs were characterized by determining the λ_{LSPR} extinction peak in air. As shown in **Figure 6**, functionalization of Au TNPs with PEG60-SH results in 60 nm red-shifts of the λ_{LSPR} extinction peak in air. This red-shift is due to a combination of the change in local refractive index of Au TNPs and the formation of the Au-S bond, which is further supported by the broadening of the LSPR dipole peak.[30,42] To validate our hypothesis and to prepare large scale, homogeneous self-assembly of Au TNPs for the SERS-based, ultrasensitive drug analysis, we studied the constant contact radius (CCR) and constant contact angle (CCA) mode-controlled droplet evaporation-based self-assembly of PEG60-S-coated Au TNPs.[43] Effective TNP-TNP, TNP-suspension, and droplet-solid support interactions are important for the formation of a 3D nanoplasmonic superlattice.[44] PEG60-S-coated Au TNPs provide efficient TNP-TNP interactions. Furthermore, the hydrophilic nature of the PEG60 chains[45,46] generate steric stabilization of the Au TNP as well as a short-range repulsive hydration force, which together induce the formation of a nanoplasmonic superlattice. In order to achieve effective droplet-solid support interactions, we investigated three different solid supports, APTES-, PHTMS-, and OCTMS-modified silicon wafers.

The contact angle for water droplets on APTES-, PHTMS-, and OCTMS-modified silicon wafers is determined to be 58, 73, and 90º, respectively, see **Figure 7**. Importantly, the contact angle values are significantly lowered for the aqueous colloidal solution of PEG60-S-coated Au TNPs

(**Figure 5 and 7**). We believe this is due to an effective droplet-substrate interaction. The contact angle data agree with the hydrophilic nature of APTES due to the presence of the terminal

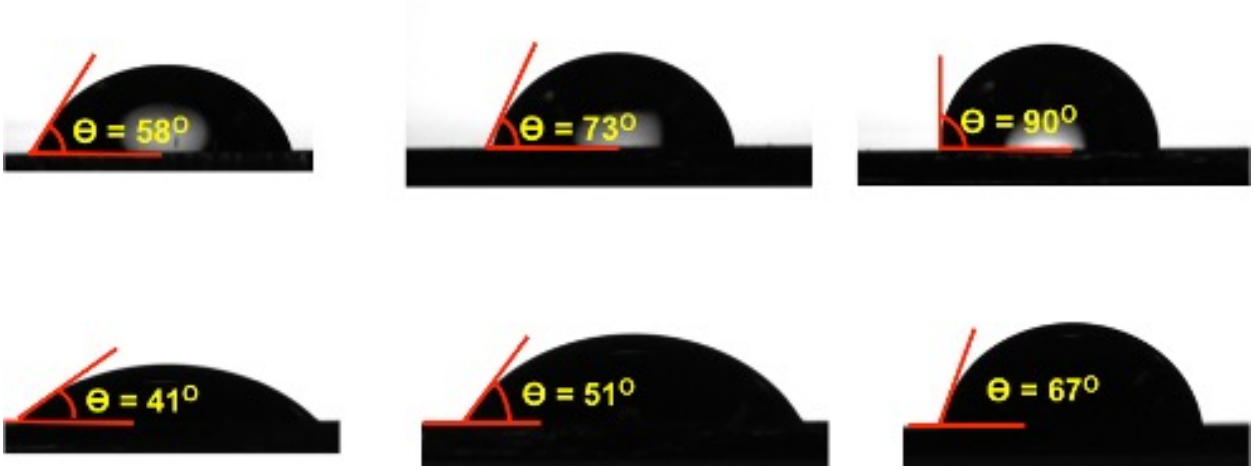

Figure 7. Contact angle images for the water droplet on (A) APTES-, (B) PHTMS-, and (C) OCTMS-modified glass supports. Contact angle images for an aqueous colloidal solution of PEG60-S-functionalized Au TNPs droplet on (D) APTES-, (E) PHTMS-, and (F) OCTMS-modified Si wafer. Adapted from Sardar et al. Analyst 2020.

–NH_2 group, where as an OCTMS support containing long aliphatic chains produces a hydrophobic surface. We conducted scanning electron microscopy (SEM) analysis to determine the spatial arrangement of PEG60-S-functionalized Au TNPs onto the above-mentioned, modified silicon wafer supports. As shown in **Figure 8A-C**, PEG60-S-coated Au TNPs form 2D, mixture of 2D and 3D, and 3D assemblies on APTES-, PHTMS-, and OCTMS-modified silicon wafers, respectively, which were used to control droplet-substrate interactions. Herein, for the SERS-based drug analysis, we refer to the nanoplasmonic superlattices prepared with APTES-, PHTMS-, and OCTMS-modified silicon wafers as **Substrate-1, Substrate-2, and Substrate-3**, respectively. Most importantly, OCTMS-modified silicon wafers produce a large-area (> 25 μm^2) self-organization of PEG60-S-coated Au TNPs, as shown in the SEM image (**Fig. 8C**). We believe that the hydrophilic character of the APTES-modified glass support promotes CCR modes. Here, the droplet evaporates with a constant area and reduces the contact angle resulting in a 2D assembly with many vacant spots. In contrast, the less hydrophobic PHTMS-modified silicon wafer provides both CCR and CCA modes during droplet evaporation. This causes the formation of short-range 3D along with 2D assemblies. Finally, CCA mode is more prominent for the OCTMS-modified silicon wafer in which the contact line disappears towards the center. This process allows the arrangement of Au TNPs in uniform staking through thermodynamically-controlled hydrophilic-hydrophilic and van der Waals interactions between polyethylene glycol chains that together result in the formation of the 3D nanoplasmonic superlattice. We characterized the optical properties of these substrates using UV-Vis-NIR spectroscopy (**Figure 8D**). The LSPR dipole peak maxima (λ_{LSPR}) of Au TNPs in Substrate-1, 2, and 3 were found to be 937, 969, and 988 nm, respectively. A progressive red-shift of λ_{LSPR} is in agreement with the plasmonic properties of electronically interacting metallic nanostructures.[47] In the 3D assembly shown in Substrate-3, a near-field plasmonic coupling between close-packed Au TNPs is

expected to be strong in comparison to either 2D or a mixture of 2D and 3D assemblies. While this does not emphasize the detailed studies that were conducted to optimize the surface ligand chemistry of Au TNPs in order to achieve 3D superlattices, we have observed that the chain length of PEG units plays an important role in the overall assembly process. Particularly, we do not observe the formation of a large area 3D nanoplasmonic superlattices with shorter glycol units such as PEG18 (data not shown). This could be due to ineffective droplet-solid support interactions.

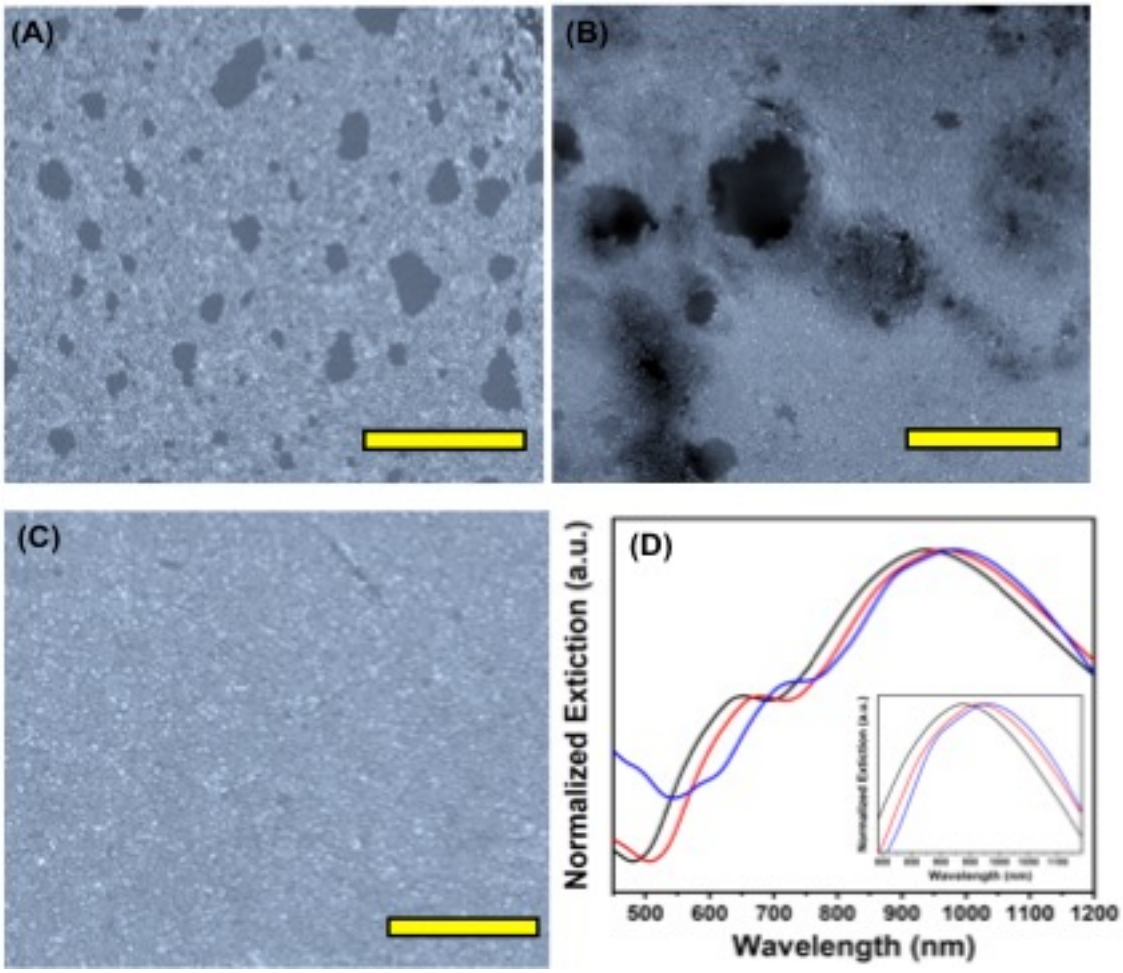

Figure 8. Low magnification scanning electron microscopy image of nanoplasmonic superlattice substrates prepared on (A) APTES- (B) PHTMS- (C) OCTMS-modified silicon wafer. Scale bars are 1.0 μm. (D) Normalized UV-Vis-NIR extinction spectra of nanoplasmonic superlattice substrates. The inset shows an expanded region of LSPR dipole peak of Au TNPs: Black (Substrate-1, λ_{LSPR} = 937 nm, APTES-modified silicon wafer), red (Substrate-2, λ_{LSPR} = 969 nm, PHTMS-modified silicon wafer), and blue (Substrate-3, λ_{LSPR} = 988 nm, OCTMS-modified silicon wafer). An average 51 nm red shift is observed between 2D self-assembly (Substrate-1) and 3D self-assembly (Substrate-3). For the UV-Vis-NIR analysis, glass coverslips were functionalized with APTES, PHTMS, and OCTMS to prepare nanoplasmonic superlattice substrates and the spectra were collected in transmission mode. Adapted from Sardar et al. Analyst 2020.

5.1.2. SERS Performances of Nanoplasmonic Superlattice Substrates for Ultrasensitive Drug Analysis. The potential of nanoplasmonic superlattice substrates for SERS-based ultrasensitive detection of drugs was studied. **Figure 9A-C** depict the SERS spectra of fentanyl for different concentrations (1.0 X 10^{-3} M to 1.0 X 10^{-12} M) collected using the three different superlattice substrates. The C-N stretch of fentanyl appears at 1334 cm^{-1}, which increases in intensity as the concentration increases. Importantly, when **Substrate-2 and -3** were used for SERS analysis, all the characteristic peaks of fentanyl can clearly be observed, even at concentrations down to 100.0 X 10^{-12} M with a signal-to-noise ratio of 3.3. We determined the limit of detection (LOD) by plotting the intensity of C-N stretch vs. logarithm of fentanyl concentration (**Figure 9D)**. The LOD for **Substrate-1, -2, and -3** were determined to be 160 parts-per-trillion (ppt), 14.9 ppt, and 130 ppq, respectively. Moreover, a wide linear dynamic range spanning 7 orders of magnitude was observed for **Substrate-2 and -3**. The SERS sensitivity of our 3D nanoplasmonic superlattice substrates is at least 5 orders of magnitude higher than other Au or Ag nanostructure-based substrates for the detection of synthetic opioids.[35] This unprecedentedly low LOD is due to the formation of a large number of electromagnetic hot spots that originate from the near-field plasmonic coupling between adjacent Au TNPs within the 3D superlattice substrate. The number of hot spots is expected to be lower in **Substrate-1** (only 2D assemblies) and **-2** (mixture of 2D and 3D assemblies). It is important to mention that we independently analyzed each superlattice substrate by SEM to confirm the assembly-type before performing SERS analyses.

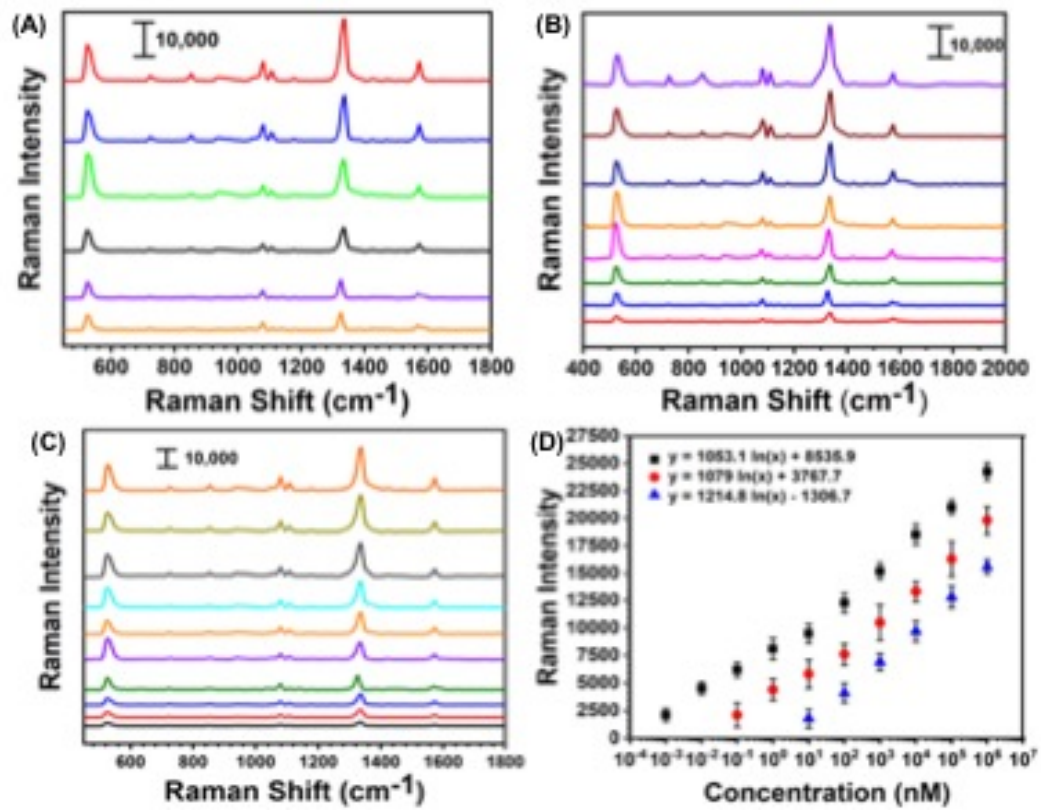

Figure 9. SERS spectra of fentanyl collected from (A) 1.0 mM to 10 nM concentrations using Substrate-1, (B) 1.0 mM to 100 pM concentrations using Substrate-2, and (C) 1.0 mM to 1.0 pM

concentrations using Substrate-3. (D) Fentanyl C-N stretch at 1334 cm^{-1} vs. log concentration for three different substrates: Blue diamonds (Substrate-1, R^2 = 0.9983), Red dots (Substrate-2, R^2 = 0.9829) and Black squares (Substrate-3, R^2 = 0.9899). Average SERS intensity was determined from 6 measurements. Adapted from Sardar et al. Analyst 2020.

In literature, polymer-coated gold nanorods (Au NRs) have been self-assembled into 3D nanoplasmonic superlattices for various SERS-based analyte detection, including drug analysis.[48] However, to the best of our knowledge, this is the first example where a 3D nanoplasmonic superlattice is prepared using a controlled droplet evaporation method of chemically-synthesized Au TNPs. For SERS-based analyte detection, TNPs are a better choice than NRs because the sharp tips and edges of TNPs induce very high electromagnetic (EM)-field enhancement in comparison to NRs, which lack such unique structural features. The EM-field could couple in near-field in a 3D superlattice producing a large number of hot spots and thus would enormously increase the SERS enhancement factor. To validate our statement, we calculated the analytical enhancement factor (AEF) of the 3D nanoplasmonic superlattice (**Substrate-3**) because it provided the most sensitive fentanyl detection. We opted to determine the AEF instead of standard SERS EF[49] because in a 3D superlattice, most of the drug molecules are expected to penetrate inside the porous 3D structures distributing throughout the superlattice volume within a confined space, as similar to a fully-dissolved analyte solution. Under this circumstance, there will be no real flat area on the SERS substrate. We calculated AEF of **Substrate-3** using a literature procedure:[50]

$$AEF = (\frac{I_{SERS}}{I_{RS}})(\frac{C_{RS}}{C_{SERS}})$$

Here, we utilize the ratio between the SERS intensity (I_{SERS}) and the normal Raman intensity (I_{RS}) for a selected concentration of fentanyl under identical experimental conditions. The I_{SERS} is 6209 for the 1334 cm^{-1} peak at 10^{-10} M concentration on the 3D nanoplasmonic superlattice, and the I_{RS} is 97 at 10^{-3} M concentration on a non-functionalized silicon wafer (**Figure 10**). We determined an AEF value of 6.4 x 10^8 AEF for **Substrate-3**. This is the highest AEF value reported for Au TNPs.[24,50] We believe this extraordinarily high AEF value is due to the unique structural features of Au TNPs and their strong near-field plasmonic coupling within the 3D superlattice. Taken together, this extraordinarily high AEF value is in agreement with the unique structural features of Au TNPs and their strong near-field plasmonic coupling within the 3D superlattice that together allow ultrasensitive analyte detection capability under this unique spatial organization.

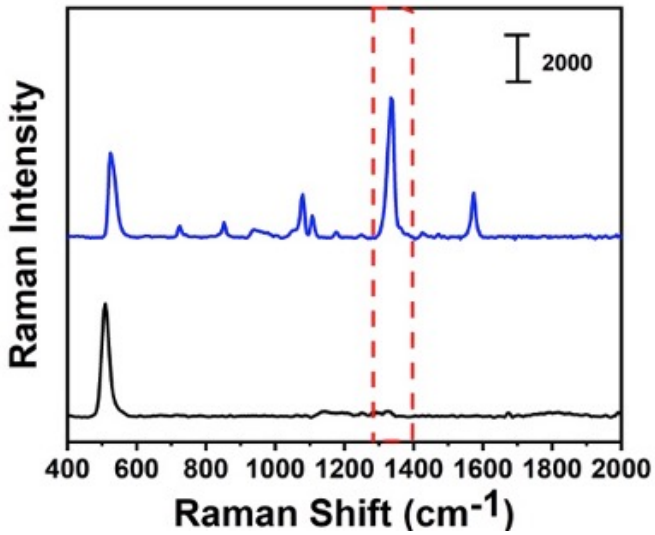

Figure 10. Black curve represents the normal Raman spectrum of 1.0 mM fentanyl on silicon wafer. Blue curve represents the SERS spectrum of 100 pM fentanyl on Substrate-3. For the AEF calculation we used C-N stretch of fentanyl at 1334 cm^{-1} as shown in the dotted red box. Adapted from Sardar et al. Analyst 2020.

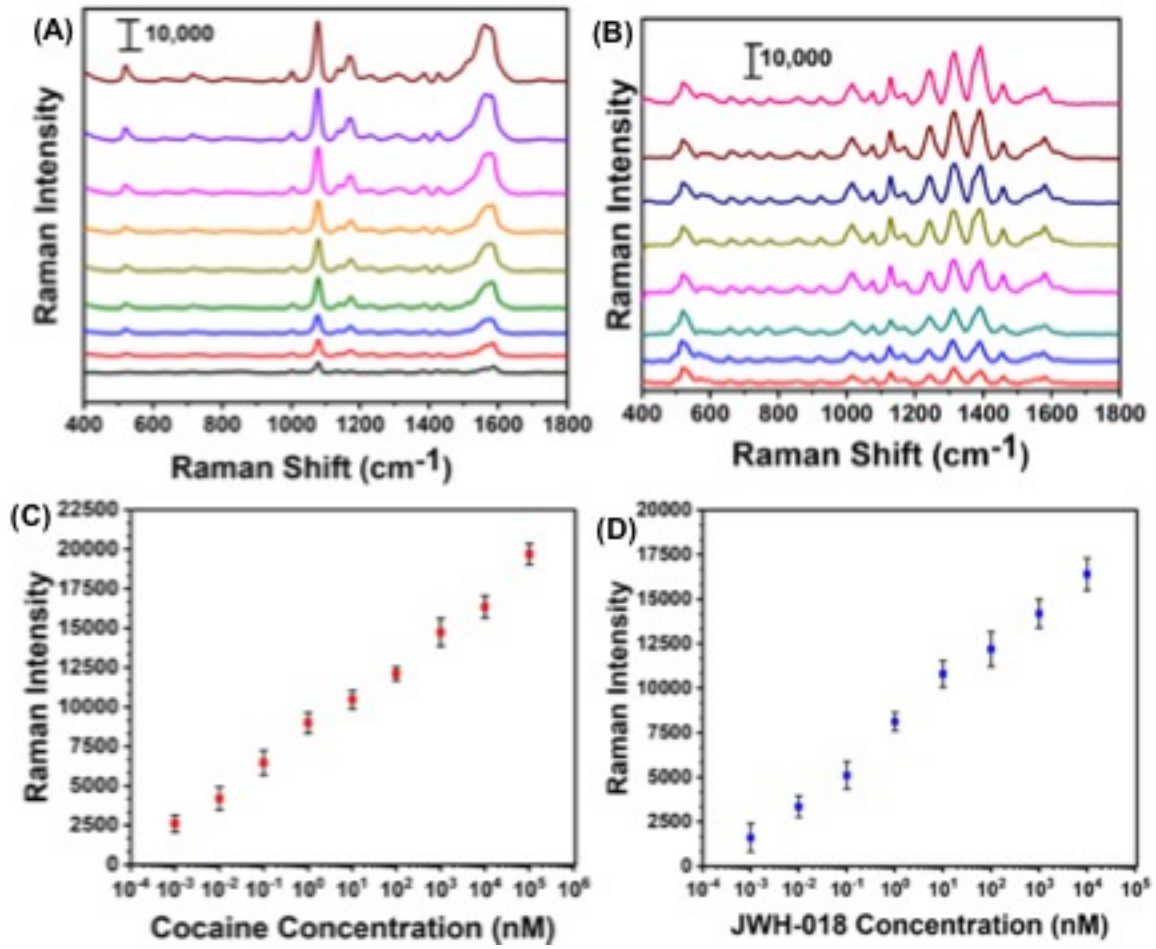

Figure 11. SERS spectra of (A) cocaine and (B) JWH-018 collected using Substrate-3. The plot of SERS intensity as a function of (C) aromatic C=C stretch at 1586 cm^{-1} of cocaine (D) naphthalene C-H stretch at 1393 cm^{-1} of JWH-018 vs. respective logarithm concentrations. Adapted from Sardar et al. Analyst 2020.

Toxicological drug analysis requires identification and quantification of different drug types and thus, any newly developed sensors should demonstrate a good versatility. The above experimental results suggest that **Substrate-3** is the most effective SERS substrate for ultrasensitive drug analysis. Therefore, we used this substrate to perform SERS analysis of two important classes of drugs, a coco alkaloid (cocaine) and a synthetic cannabinoid (JWH-018). We selected these drugs because they are highly potent and/or most abused in the United States.[51] Furthermore, the use of a mixture of cocaine and cannabinoid significantly increases the mortality risk compared to other drug mixtures seen in ED patients.[52] **Figure 11A-D** show concentration dependent SERS spectra and the corresponding calibration plots for cocaine and JWH-018. We used the aromatic ring (C=C) stretch at 1586 cm^{-1} for cocaine and naphthalene C-H stretch at 1393 cm^{-1} for JWH-018 to develop calibration plots. Impressively, we are able to quantify cocaine and JWH-018 at a LOD of 32.3 and 118.9 ppq, respectively, with an excellent linear dynamic range. Our LOD value for cocaine is well under the concentration of a positive test guideline issued by the United States Department of Health and Human Services.[53] Reproducibility of the

SERS response is crucial for forensic toxicology applications. To study reproducibility in the fabrication of nanoplasmonic superlattices for SERS applications, we synthesized four different batches of Au TNPs, and fabricated four **Substrate-3** from each batch of Au TNPs (n = 16). We measured the SERS of 1.0 μM fentanyl. As shown in **Figure 12**, only 3.8% relative standard deviation is observed amongst 16 superlattice substrates in SERS analysis. The data confirm that our fabrication strategy is highly reproducible.

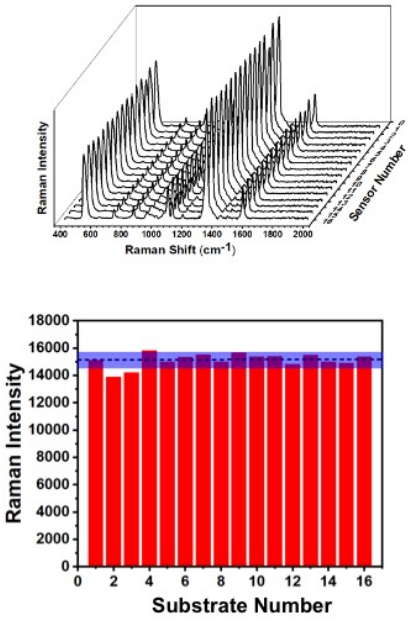

Figure 12. (Top) The reproducibility of our developed nanoplasmonic superlattice for SERS-based drug analysis. SERS spectra of 1.0 μM fentanyl were collected from 16 different substrates. **(Bottom)** The bar graph shows relative standard deviation of 3.8% amongst 16 superlattices. Adapted from Sardar et al. Analyst 2020.

.

5.1.3. Correlating Experimentally-Determined SERS Spectra of Drugs with Theoretical Calculations. It is important to discuss that the SERS spectra we acquired for fentanyl using our nanoplasmonic superlattice substrates are different than those reported in the literature.[35,54] One of the drawbacks in the current literature reporting SERS-related drug detection is that each article assigns Raman stretches of drug molecules based on the convenience without any additional support for such a selection.[12,35,45,48,55] For an example, literature report on DFT calculations of just fentanyl molecules showed that the aromatic C=C stretch would be much higher in intensity that the H-C-N2 stretch.[56] In contrast, as shown in **Fig. 9**, fentanyl displays higher intensity H-C-N2 Raman stretch (~1340 cm^{-1}) than the aromatic C=C stretch (~1000 cm^{-1}). Therefore, we used H-C-N2 stretch to develop the calibration plot as opposed to commonly used aromatic C=C stretch.[35,54]

It has also been reported in the literature that electronic interactions between analyte molecules and metal nanostructures shifts Raman vibration modes;[21] however, to our knowledge, no report is available demonstrating this unusual variation in Raman peak intensity. As shown in **Figure 13A**, the SERS spectrum of fentanyl collected using our 3D nanoplasmonic superlattice substrates closely resembles the DFT-calculated spectrum in which N2 of fentanyl molecule electrostatically interects with a Au atom. It is known that thiolated ligands bind onto low index facets of Au nanostructures, whereas high index facets such as sharp corners and edges remain unpassivated.[57] Therefore, we hypothesize that PEG60-thiolates coat the flat surface of Au TNPs leaving sharp tips and corners unpassivated where drug molecules could electrostatically adsorb due to strong Au-N interactions.[21] It is also known that direct adsorption/attachment of analyte molecules onto plasmonic metal nanostructures increases the SERS enhancement.[49] We observed a slight shift in Raman peak position between experimental acquired spectrum and DFT-calculated spectra. This could be due to the variation in the orientation of fentanyl molecule adsorbed onto the TNP surface.[20] Finally, one could argue that thick PEG60-S-coating would lead the drug molecule to directly adsorb onto the polymer layer. To overrule such possibility, we also

acquired DFT-calculated Raman spectra of fentanyl hydrogen-bonded with the oxygen from glycol unit. Interestingly, the Raman stretch and/or peak intensity are almost identical with pure fentanyl molecule. Therefore, we believe that the hydrophilic character of PEG60 repels highly hydrophobic fentanyl molecules that could prompt them to diffuse through the porous 3D structure of plasmonic superlattice substrates and bind with exposed Au atoms of TNPs. We also conducted DFT calculations for cocaine and JWH-018 and the data strongly support the formation of Au-N interaction (**Figure 13B**). Taking our TDDFT data into consideration, the excellent LOD for fentanyl, cocaine, and JWH-018 is in agreement with unique structural properties of our developed 3D nanoplasmonic superlattice substrates for SERS analysis. Additional DFT-calculated Raman spectra (**Figure 14**) and the vibrational modes of calculated Raman stretches (**Table 1**) are provided in the supporting information file.

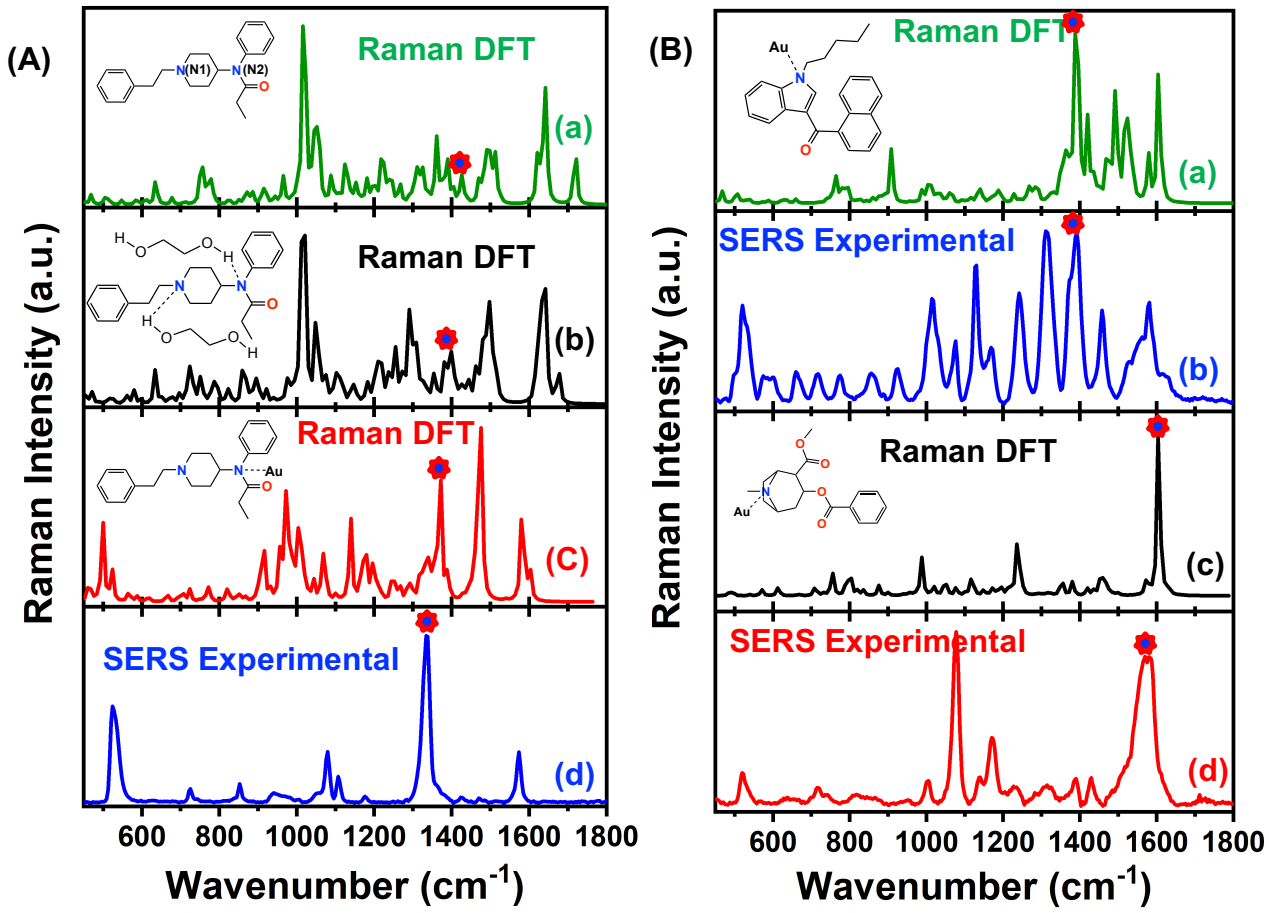

Figure 13. (A) Comparison of DFT-calculated Raman spectra of fentanyl under different molecular interactions: (a) only fentanyl, (b) fentanyl hydrogen-bonded with ethylene glycol, (c) N2 of fentanyl electronically interacting with a Au atom and (d) experimenatlly-acquired SERS spectra using Substrate-3. Asterisks represent the position of H-C-N2 Raman stretch of fentanyl. (B) DFT-calculated Raman spectra of Au-attached JWH-018 (a) and cocaine (c), and experimental SERS spectra of JWH-018 (b) and cocaine (d). Asterisks represent position of naphthalene C-H stretch of JWH-018 and aromatic C=C stretch of cocaine. Adapted from Sardar et al. Analyst 2020.

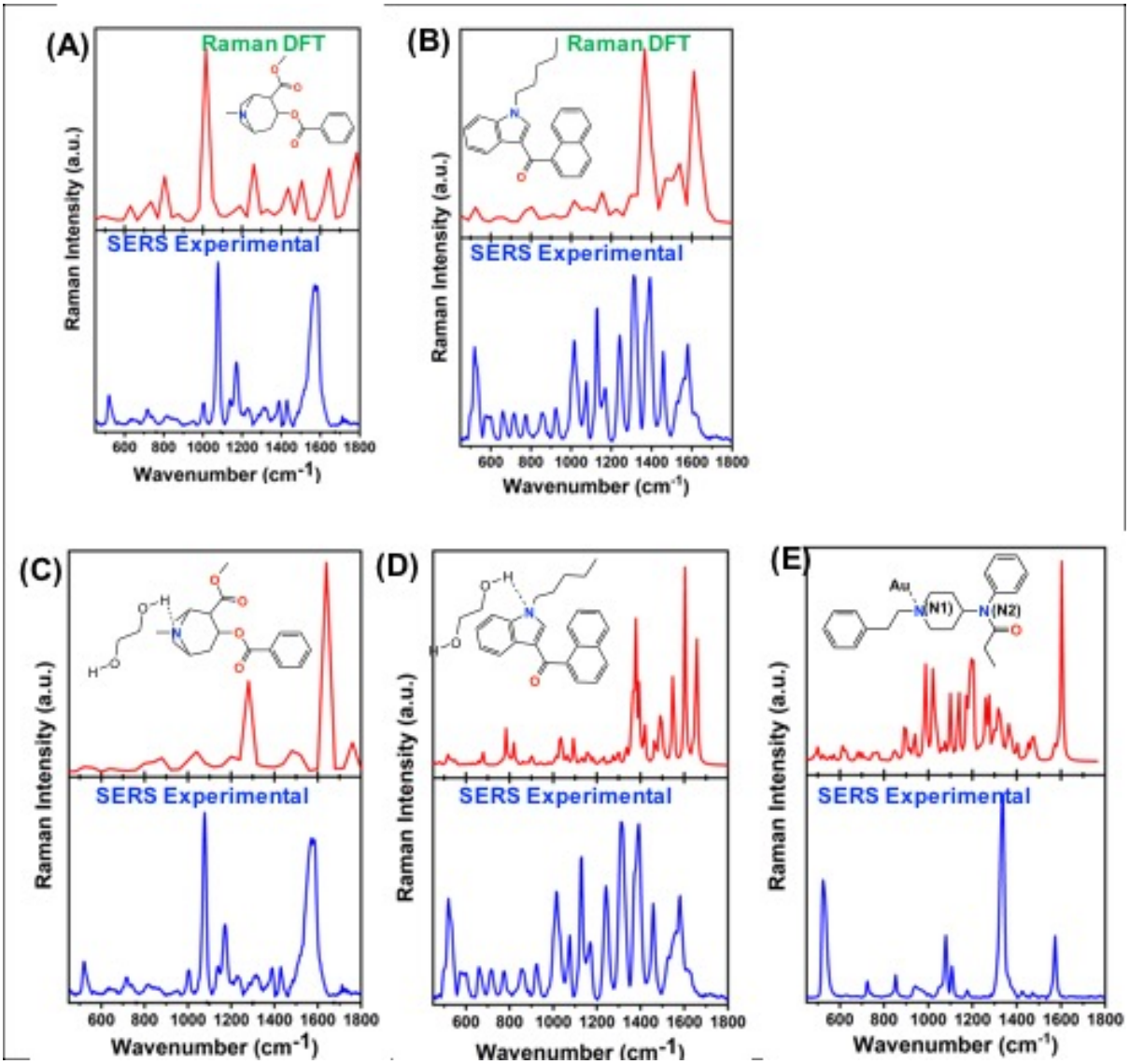

Figure 14. DFT-calculated Raman spectra of cocaine (A) and JWH-018 (B). Experimental SERS spectra (blue curve) and DFT-calculated Raman spectra (red curve) of (C) cocaine, (D) JWH-018, and (E) fentanyl in which their nitrogen atom formed hydrogen bonding with ethylene glycol. Adapted from Sardar et al. Analyst 2020.

5.1.4. SERS-Based Real Toxicological Plasma Sample Analysis from the Emergency Department Drug-of-Abuse (DOA) Patients. Impact of a new laboratory-based analytical technique can only be evaluated by testing potential applications in real world samples. In clinical toxicology, standard immunoassay analysis is routinely performed to determine the type of drugs that patients have consumed. However, inadequate sensitivity in most immunoassay techniques cause them to fail at detecting synthetic cannabinoids and opioids. Thus, for proof-of-concept, we

analyzed 10 samples of DOA patient plasma from the ED using the SERS technique. For the patient sample analysis, first the crude plasma samples were diluted with RNA-free water to prepare a 10% plasma solution. From this, a total 6 µL of sample was drop-casted onto **Substrate-3** (prepared using OCTMS-functionalized glass support). **Figure 15A** shows the SERS spectra from six patients' plasma, in which we are able to determine that the plasma of patients-(a) and (b) contained cocaine, and patients-(d), -(e), and –(f) contained fentanyl. Most importantly, the plasma of patient-(c) contained both cocaine and fentanyl (**Figure 15B**). We independently confirmed the identity of the drugs in patients-(a) to (f) using our novel paper spray ionization (PSI)-mass spectrometry (MS) technique (data not shown). Utilizing the calibration plot developed for fentanyl (**Figure 9D**) and cocaine (**Figure 11C**) for **Substrate-3**, we also determined the concentration of drugs in the-above mentioned six samples. Taken together, our SERS-based drug analysis shows an excellent selectivity, which is a key requirement in clinical samples for court admissible data. Perhaps, our SERS-based drug detection approach can be implemented to analyze real-world forensic toxicology samples.

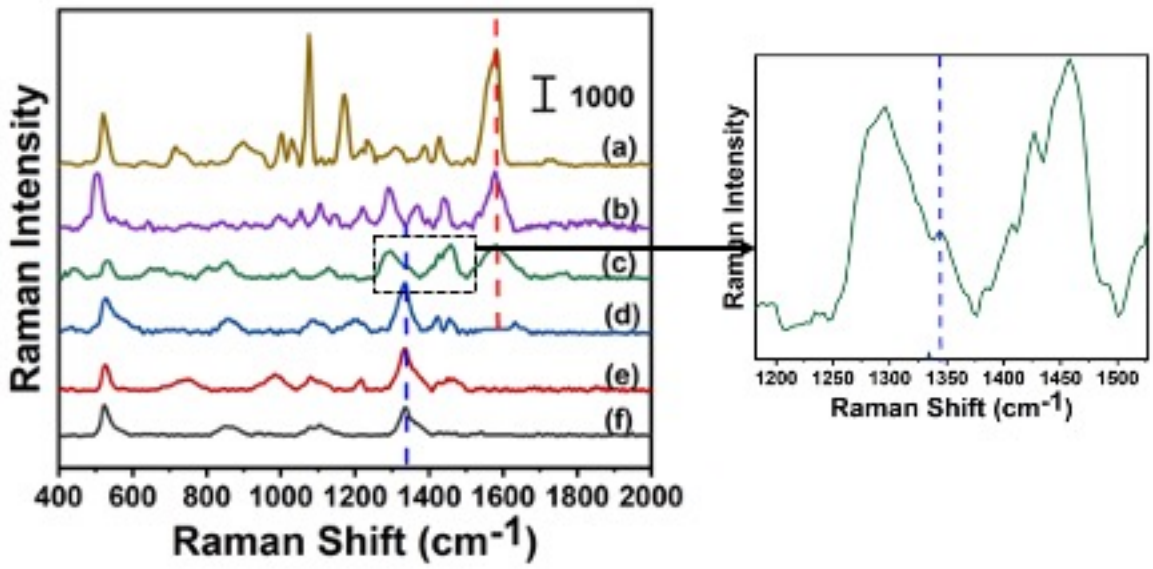

Figure 15. SERS spectra of six-patient plasma diluted to 10% (v/v) with RNase free water and then drop-casted onto Substrate-3 for analysis. The blue and red dashed lines represent the peak corresponding to C-N stretch at 1334 cm^{-1} of fentanyl and C=C stretch at 1586 cm^{-1} of cocaine, respectively. An expanded spectral area of patient-(c) sample is shown in (B). The blue dashed line is representing the peak assigned to C-N stretch at 1334 cm^{-1} of fentanyl. Adapted from Sardar et al. Analyst 2020.

5.1.5. Summary. In summary, a solid-state fabrication strategy was developed to prepare nanoplasmonic superlattice substrates by controlling the self-assembly process of polymer-coated Au TNPs to create ultrasensitive detection of potent drugs in human plasma using the SERS technique. This nanoplasmonic superlattice substrate provides several advantages over traditional SERS-based techniques: (1) The thermodynamically-controlled formation provides homogeneous assembly and produces a highly reproducible SERS signal. (2) The porous 3D structure allows analytes to enter inside the superlattice structures, possibly within a close vicinity of the electromagnetic hot spot for the maximum SERS signal. In contrast, traditional SERS-

based techniques rely on analyte adsorption onto the top surface of the substrate, in which hot spots may or may not be present. (3) As mentioned before, PEGs are known to reduce non-specific adsorption of endogenous biomolecules from biofluids, and therefore increase selectivity, as we have observed in this study. Our DFT calculations also support the unique structural properties of the superlattice substrate that resulted in an exceptionally high SERS sensitivity. We believe that our newly developed 3D nanoplasmonic superlattices could advance forensic toxicology applications by analyzing potent drugs directly from the plasma samples of DOA samples using a label-free SERS technique. Although we have demonstrated the utility of our nanoplasmonic superlattice substrates in toxicology drug analysis, the substrates could also be used for ultrasensitive SERS-based detection and quantification of any analytes such as pesticides, explosives, radioactive materials, and biomolecules both in aqueous medium and human biofluids.[58-62]

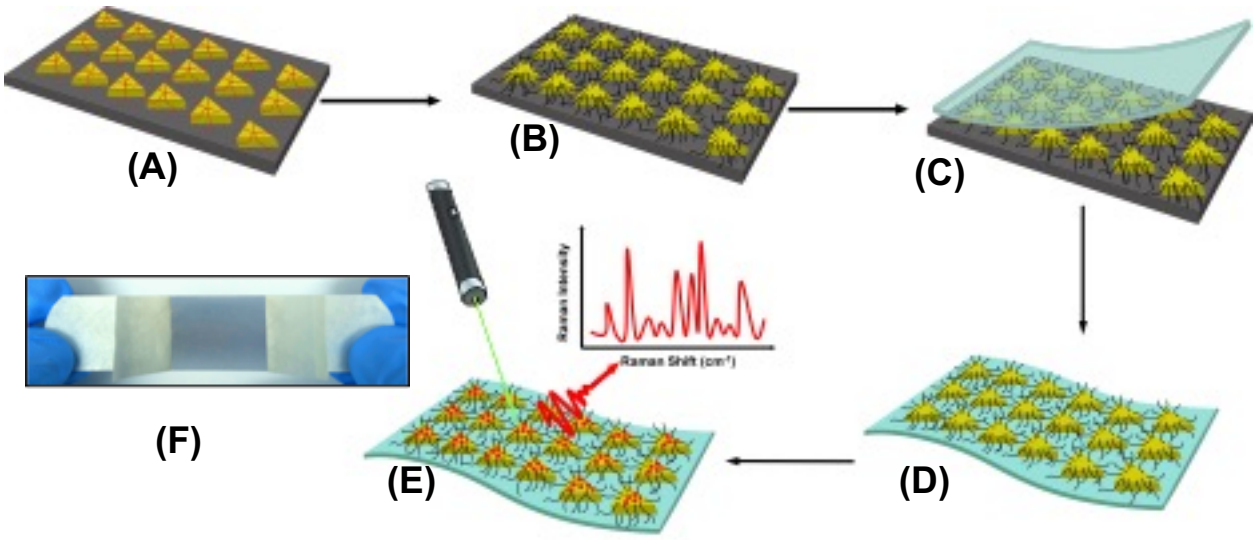

Figure 16. Schematic represent of the fabrication process for our SERS plasmonic patch as follows: Chemically synthesized Au TNPs in acetonitrile are immobilized onto an APTES-functionalized glass substrate through incubation to form a self-assembled layer of TNPs (A), which avoids unwanted aggregation of Au TNPs and results in reproducible nanosensors fabrication. Au TNPs are then functionalized with polyethylene glycol-thiolate (B) to enhance specificity. 3M adhesive tape is placed on the Au TNP-containing glass substrate, pressed gently with the thumb, and removed at a 90^0 angle (C) which results in successful lift-off of the Au TNPs from the glass to the tape, producing the plasmonic patch (D). A 6.0 microliter human biofluids can be drop-casted directly onto the nanosensor (D) which results in physisorption of drugs onto TNPs (E). SERS spectra then collected using a Raman spectrometer with 785 nm laser excitation. (F) The bluish gray area in the photograph is the plasmonic patch and the overall construct resembles with Band-Aid.^{TM} Adapted from Sardar et al. Anal. Chem. 2021.

5.2. Flexible SERS Substrates for Toxicological Drug Analysis. The research described above shows the importance about the self-assembly of metallic nanoparticles in SERS. To further demonstrate the unique aspects of our SERS-based toxicological drug analysis, we

pursued to construct a simple SERS nanosensor fabrication strategy that meets both of the above-mentioned requirements to achieve high sensitivity and specificity, while mitigating fouling effects. Here, we used Au TNPs as plasmonic nanostructures in the SERS nanosensor fabrication. We adopted a two-step fabrication strategy: Firstly, functionalize Au TNPs with PEG-S- to avoid non-specific adsorption of endogenous biomolecules and thus provide excellent non-fouling effects. Secondly, use transparent adhesive tape as a flexible substrate to immobilize PEG-S-functionalized Au TNPs to create large number of EM hot spots. Together, our fabrication strategy produces "self-assembled" monolayers of PEG-S-functionalized Au TNPs onto a transparent and flexible adhesive tape support, which we refer to as "plasmonic patch" for the SERS-based drug analysis. The fabrication strategy is schematically shown in **Figure 16** and described below: (1) Freshly prepared, TEA-passivated chemically synthesized Au TNPs are physiosorbed onto APTES-functionalized glass coverslips via solution phase incubation. A weak intermolecular interaction between TNP-bound TEA and APTES allows physisorption. (2) The surface of TNPs is functionalized with PEG60-SH via ligand exchange chemistry. A soft acid (Au)-soft base (S) interaction easily replaces weakly adsorbed amine ligands from the surface of Au nanostructures.[63] (3) 3M adhesive tape is placed onto PEG60-S-functionalized Au TNPs, gently pressed, and then removed slowly to transfer TNPs from the glass support onto the flexible adhesive substrate.

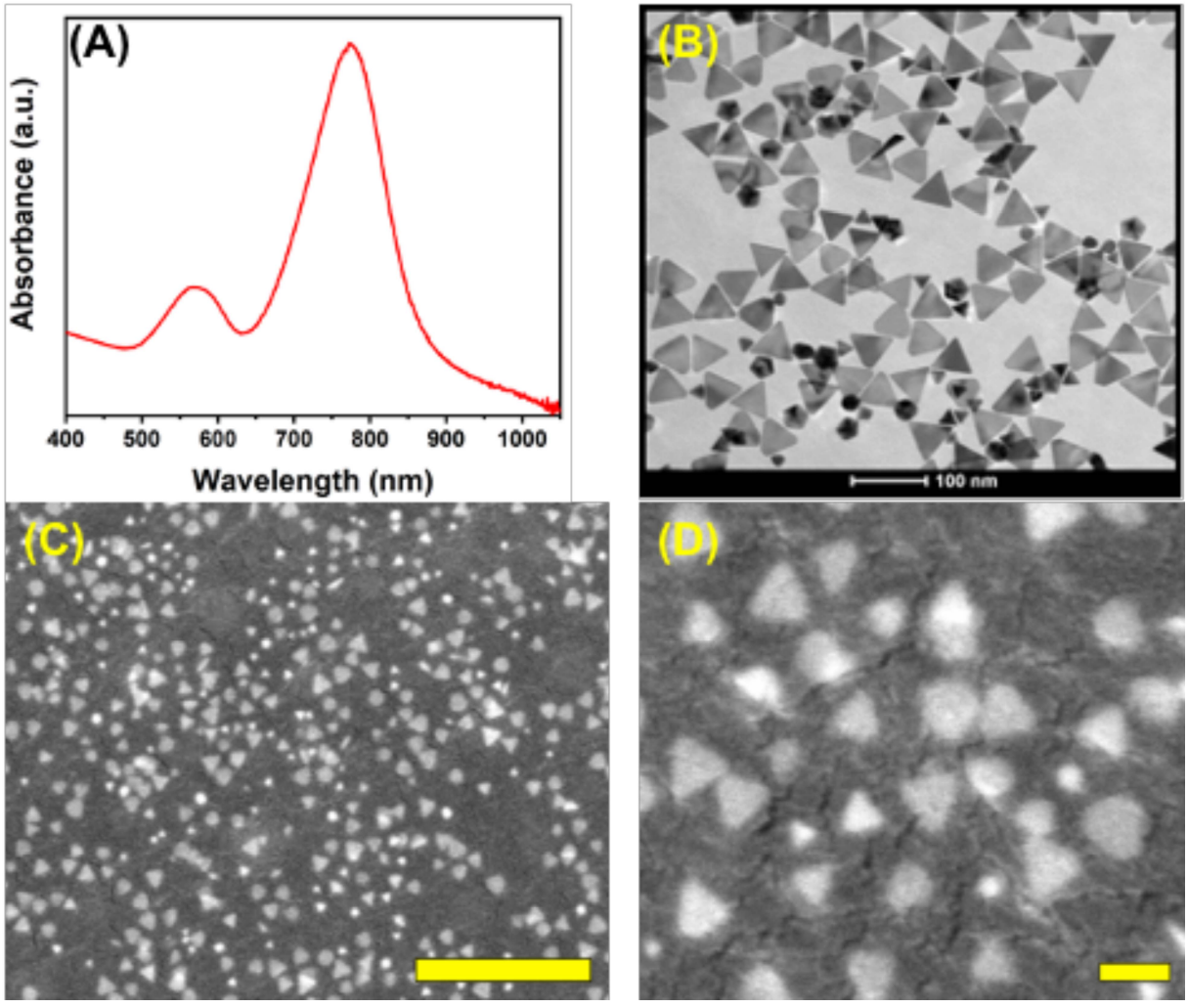

Figure 17. Spectroscopy and microscopy characterizations of Au TNPs and the plasmonic patch. (A) A representative UV-vis absorption spectrum of freshly synthesized TEA-passivated Au TNPs, which display an LSPR dipole peak (λ_{LSPR}) at 795 nm in acetonitrile. (B) A representative TEM micrograph of Au TNPs. (C) A low magnification SEM image of a plasmonic patch showing self-assembled, PEG-thiolate-functionalized Au TNPs onto 3M adhesive tape. Scale bar is 500 nm. (D) A high magnification SEM image of a plasmonic patch. No structural deformation of Au TNPs is observed even after adsorption onto the adhesive tape. Scale bar is 50 nm. Adapted from Sardar et al. Anal. Chem. 2021.

We used Au TNPs because of their unique structural and LSPR properties. Au TNP contains multiple sharp tips and edges that allow a strong electromagnetic field enhancement due to the formation of SERS hot spots.[64] Strong Au-S bonds are expected to provide long-term stability of the plasmonic patch, specifically in human biofluids. Atomically flat surface of TNPs should induce homogeneous ligand packing, resulting in the improvement of non-specific adsorption of biomolecules from human biofluids and thus less fouling effects.[27] The synthesis of Au TNPs is conducted by a colloidal reduction method of organometallic gold salt by polymethylhydrosiloxane in acetonitrile.[11,28,30,65] We used TEA to control the nucleation and growth processes for the formation of TNPs. **Figure 17A** illustrates a UV-visible absorption spectrum of Au TNPs exhibiting a characteristic LSPR dipole peak at ~795 nm in acetonitrile.[29,42] TEM analysis shows the presence of 42 $\pm$ 6 nm edge-length Au TNPs (**Figure 17B**). Based on our reported works, the Au TNPs displaying LSPR dipole absorption peak ~795 nm in acetonitrile should have ~8 nm in thickness.[59] TEA-passivated Au TNPs attached onto the APTES-functionalized glass substrate display the LSPR dipole extinction peak at ~730 nm in air. Upon PEG60-S- functionalization and transferring from glass onto flexible substrate, the LSPR dipole peak red shifts to 820 nm (**Figure 18**). This 90 nm dipole peak red shift of Au TNPs is a combination of the formation of Au-S bonds, near-field plasmonic coupling, and the change in their local refractive index (thick PEG60 layer and adhesive polymer of 3M tape). Nevertheless, this LSPR peak position is higher in wavelength and thus suitable for the use of a 786 nm laser for the SERS analysis to enhance signal intensity.[38] As shown in **Figure 17C,D**, the plasmonic patch containing TNPs was analyzed by SEM. The image reveals uniform adsorption of TNPs with 2% surface coverage without the formation of large aggregates. Therefore, the plasmonic patch can be considered a self-assembled flexible substrate. Furthermore, TNPs are randomly oriented in their self-assembled organization onto the flexible substrate, which helps in producing accidental hot spots, overall enhancing the electromagnetic field. Importantly, adhesive tape containing an Au TNP monolayer shows bluish color and the configuration of a plasmonic patch can be replicated like a “Band-Aid” that is expected to provide long-term stability during storage (vide infra).

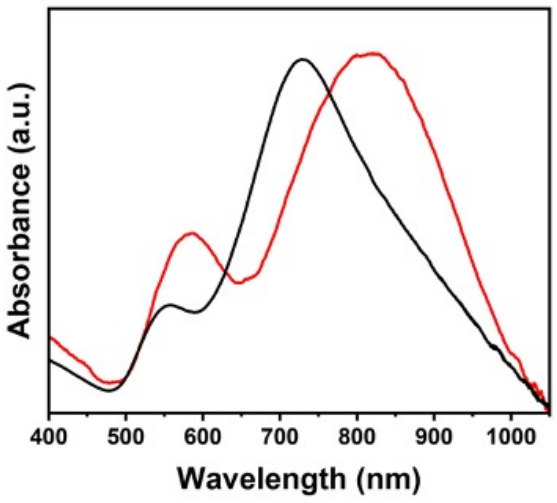

Figure 18. UV-Vis extinction spectra of different SERS-substrates. TEA-functionalized Au TNPs on APTES-functionalized glass substrate (black, λ_{LSPR} = 730 nm). PEG-60-thiolate functionalized Au TNPs on flexible adhesive tape substrate (red, λ_{LSPR} = 820 nm). Adapted from Sardar et al. Anal. Chem. 2021.

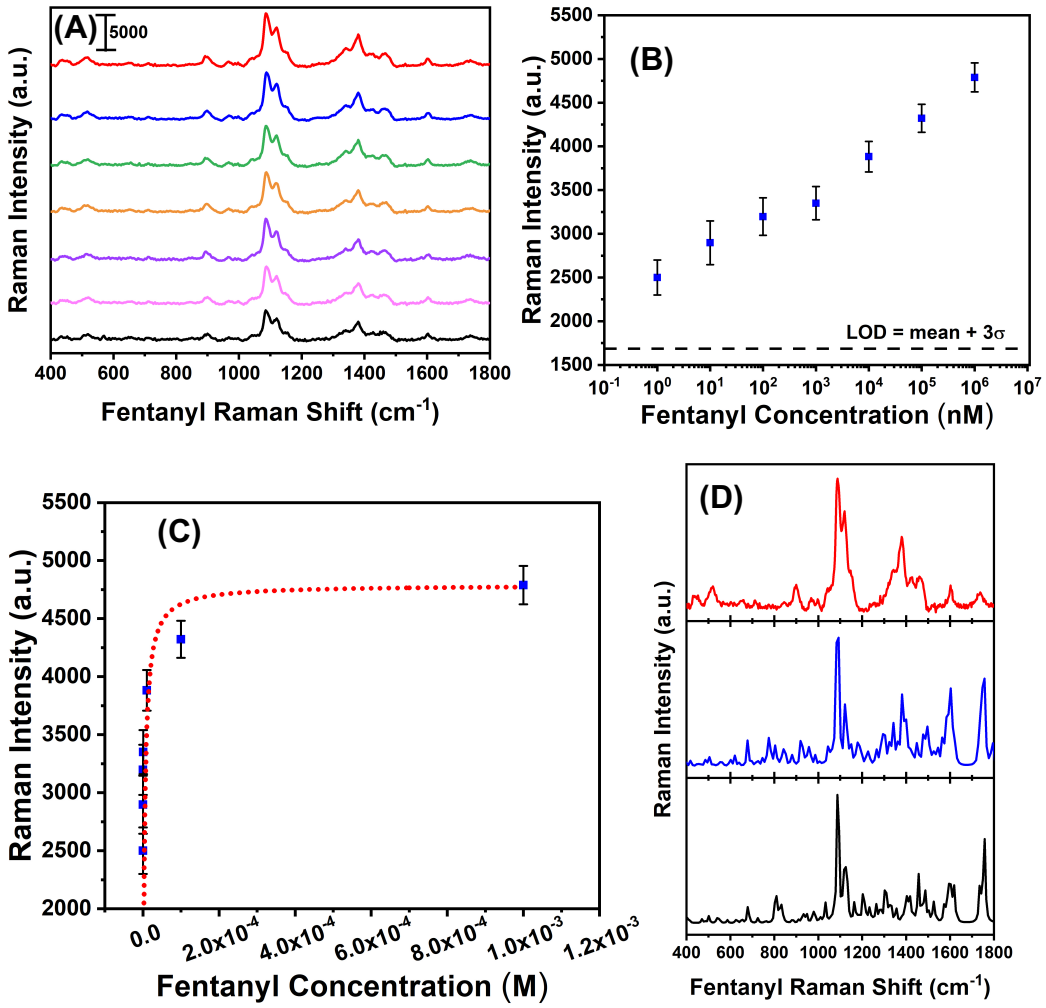

Figure 19. SERS performances of the plasmonic patches. (A) Concentration dependent SERS spectra of fentanyl collected using the plasmonic patch. (red = 1 mM, blue = 100 pM, green = 10 pM, orange = 1 pM, purple = 100 nM, pink= 10 nM, black = 1 nM). (B) The relationship between fentanyl H-C-N2 stretch as a function of log concentration. Log concentration was used to determine the background signal at the lower concentration range. Each concentration represents two different spots in three independently fabricated sensors (a total of six measurements). (C) Adsorption isotherm of fentanyl on plasmonic patch. The dotted red line is the fit to the Langmuir isotherm model. (D) A comparison of experimentally acquired SERS spectrum of fentanyl (red curve), and theoretically calculated Raman spectra of glycol bound fentanyl (blue curve) and pure fentanyl (black curve). Adapted from Sardar et al. Anal. Chem. 2021.

5.2.1. Analytical Figures of Merits of the Plasmonic Patch for SERS-Based Drug Detection. Herein we test the hypotheses that (1) plasmonic patches are expected to provide a higher SERS sensitivity in comparison to PEG60-S-functionalized Au TNPs adsorbed onto glass substrates and (2) the plasmonic patch will provide an improved non-fouling effect in comparison to TEA-passivated Au TNPs adsorbed on either glass or flexible adhesive tape in the SERS analysis. To validate our hypotheses, we compare the above-mentioned four different SERS substrates using

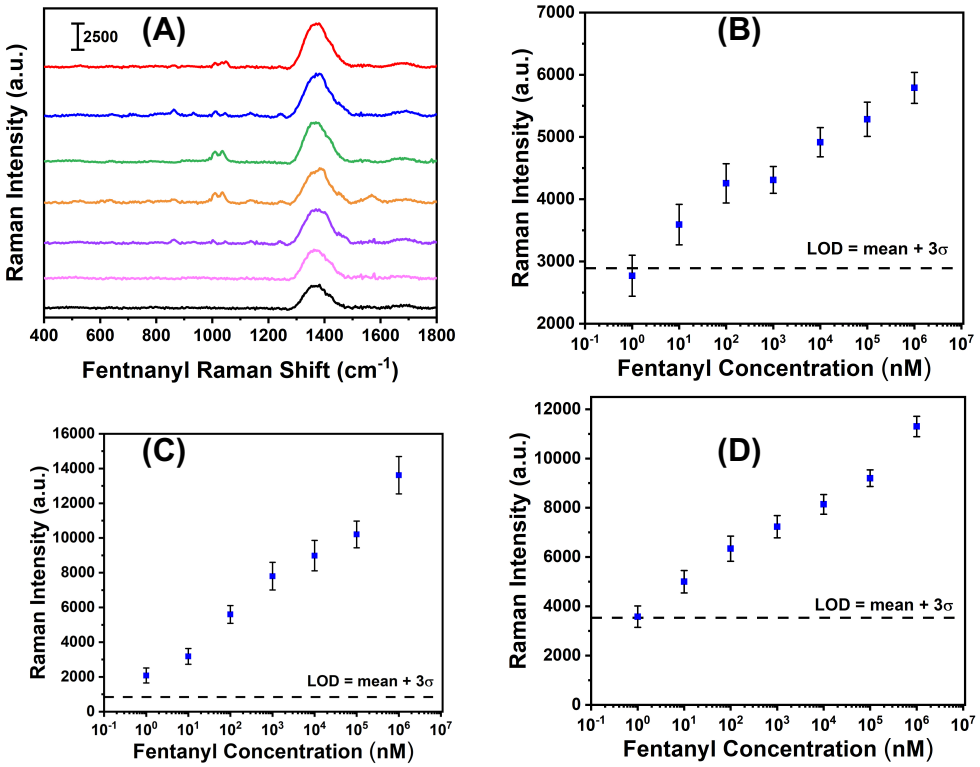

Figure 20. Concentration dependent SERS spectra (red = 1 mM, blue = 100 pM, green = 10 pM, orange = 1 pM, purple = 100 nM, pink= 10 nM, black = 1 nM), and the corresponding calibration plot (B) of fentanyl when PEG60-thiolate-functionalized Au TNPs adsorbed onto the glass were used as a substrate. Calibration plots of fentanyl SERS spectra determined when TEA-passivated Au TNPs adsorbed onto a (C) flexible adhesive substrate and (D) non-flexible glass substrate. Adapted from Sardar et al. Anal. Chem. 2021.

fentanyl as a model analyte. **Figure 19A** shows concentration dependence SERS spectra of fentanyl acquired using plasmonic patches. All the characteristic Raman stretches of fentanyl are detected in the spectrum. We used a distinct H-C-N2 stretch at 1384 cm^{-1} to determine the LOD, which is found to be 8.9 pM (3.0 picogram/milliliter (pg/mL)) (**Figure 19B**). We selected H-C-N2 for our study instead of commonly used C-C-C trigonal benzene Raman stretch of fentanyl ~1000 cm-1 because most potent drugs contain multiple aromatic rings in their structures. Therefore, it would be difficult to distinguish drugs such as fentanyl and heroin based on characteristic C-C-C Raman stretches. Instead, H-C-N2 stretch of fentanyl at 1384 cm^{-1} is distinctly unique and not

present in other drugs, thus we expect a much-improved specificity while analyzing drug mixtures, as discussed later in this article. The LOD is more than 50-fold higher than when PEG60-S-functionalized Au TNPs adsorbed onto glass substrates were used for SERS-based fentanyl analysis (LOD ~ 594.4 pM, 200 pg/mL), **Figure 20A,B**. We further determined the LODs for two additional SERS substrates, TEA-passivated Au TNPs adsorbed onto a flexible adhesive substrate (LOD = 297.2 pM, 100 pg/mL) and non-flexible glass substrates (LOD ~ 802.4 pM, 270 pg/mL), see **Figure 20C,D**. For the fentanyl detection, the LODs we determined for different plasmonic substrates are at least 100-fold better than literature reports in which spherical Ag or Ag nanoparticles were used to prepare the SERS substrates.[35,66] Clearly, the presence of sharp edges and corners of TNPs lead to a strong EM-field enhancement in our plasmonic patch that provides the higher sensitivity. In contrast, the EM-field enhancement in spherical nanoparticles is relatively low.[64] To the best of our knowledge, as mentioned above, only spherical metallic nanoparticles were used for the fabrication of SERS substrates for fentanyl detection. In this context, we are the first to demonstrate the successful implementation of anisotropic-shaped nanoparticles for fentanyl analysis using a non-flexible, three-dimensional self-assembled SERS substrate.[67] Nevertheless, we believe that the flexibility of the adhesive tape brings the TNPs closer to each other, inducing strong near-field interparticle plasmonic coupling between Au TNPs and thus creating high intensity plasmonic hot spots at the nanogap.[36]

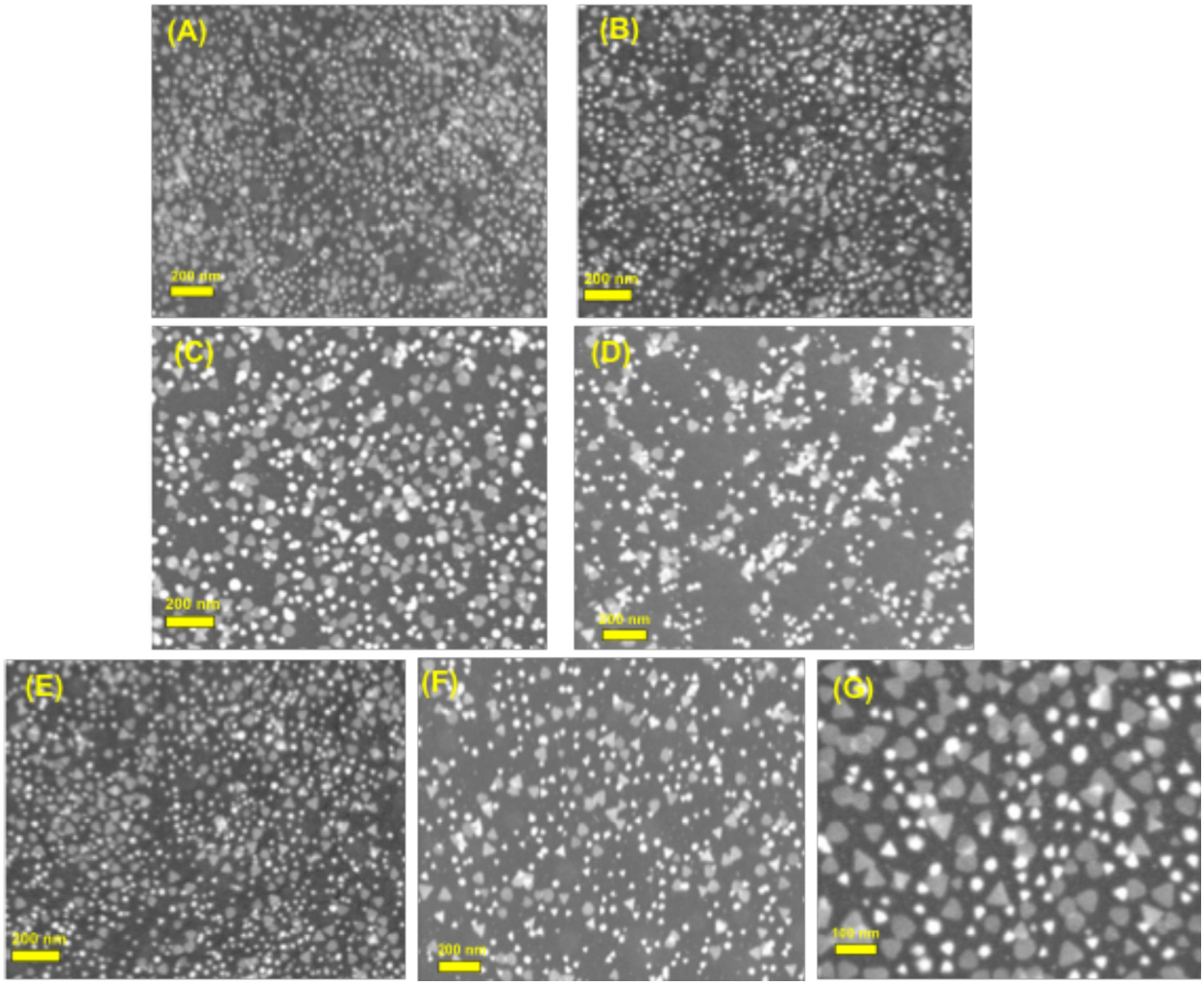

Figure 21. Representative SEM images of TEA-passivated Au TNPs adsorbed onto a flexible adhesive substrate before (A) and after (B) addition of 6 µL aqueous analyte solution, PEG60-S-functionalized Au TNPs adsorbed onto a glass substrate before (C) and after (D) addition of aqueous analyte solution, TEA-passivated Au TNPs adsorbed onto a glass substrate before (E) and after (F) addition of aqueous analyte solution, and (G) plasmonic patch after addition of aqueous analyte solution. Adapted from Sardar et al. Anal. Chem. 2021.

We also characterized different SERS substrates (TEA- and PEG60-S-functionalized Au TNPs adsorbed onto glass substrates, and TEA-passivated Au TNPs adsorbed onto a flexible adhesive substrate) by SEM to determine any possible changes in TNP organization during the solvent evaporation steps while drop casting the analyte solution (**Figure 21**). Interestingly, we observe no change in TEA-passivated TNP assembly before and after addition of analyte solution when they are adsorbed onto the adhesive tape (**Figure 21A,B**). Since TNPs are embedded inside the adhesive polymer matrix, their movement during the solvent evaporation is highly resistive. In contrast, either TEA-passivated or PEG60-thiolate-functionalized TNPs are chemisorbed onto amine terminated glass substrates via weak Au-N interactions but with an excellent two-dimensional arrangement (**Figure 21C-D**). Addition of solvent could destroy the two-dimensional self-assembly during the evaporation process. Also, TNPs could migrate onto the solid surface due to a weak Au-N interaction. This is evident from the appearance of aggregated arrangement of TNPs onto glass substrates (**Figure 21E-F**). Importantly, microscopy analysis of PEG-functionalized Au TNPs adsorbed onto adhesive tape (plasmonic patch) does not show any noticeable change in self-organized assembly of TNPs after drop-casting of the analyte solution (**Figure 21G**). Together, we believe that the enhanced sensitivity and non-fouling effects of PEG-functionalized Au TNPs onto adhesive tape (plasmonic patch) in the SERS-based drug detection is solely because of specific molecular interactions.

To further understand the substrate effect on SERS sensitivity, we determined and compared SERS EF of plasmonic patch and PEG60-S-functionalized Au TNPs adsorbed onto glass substrates using Eq. 1.

$$\text{SERS EF} = \left[\frac{I_{SERS}}{I_{NR}}\right]\left[\frac{N_{NR}}{N_{SERS}}\right] \quad (1)$$

Here, I_{SERS} and I_{NR} are SERS and normal Raman intensity of fentanyl, respectively. The N_{NR} and N_{SERS} are number of analyte molecules present in normal Raman and SERS analyses, respectively. Considering fentanyl resides flat onto the surface and TNPs cover nearly 2% of the total substrate surface, we determined SERS EF based on a literature procedure.[35] We obtain SERS EF to be 4.5 X 10^7 and 5.2 X 10^5 for plasmonic patch and PEG60-S-functionalized Au TNPs adsorbed onto glass substrates, respectively. The results are in agreement with the LOD values mentioned above and also validate our first hypothesis that a higher Raman signal enhancement would be observed when PEG60-S-functionalized TNPs were present onto a flexible substrate (plasmonic patch) than a non-flexible solid substrate (glass). The SERS EF of 4.5 X 10^7 we calculated for the plasmonic patch is comparable to Ag-based SERS substrate for fentanyl detection.[35] It is known that Ag-based substrates provide better SERS EF as compared to Au because of the low optical loss and enhanced LSPR properties.[16] However, Ag is more

prone to oxidation than Au, which makes the latter more desirable in SERS substrate fabrication. Park et al., reported one order magnitude higher SERS EF when PDMS-embedded Au nanostars, as a flexible substrate, were used for the SERS analysis.[68] The reported method requires additional Ag film substrate, as well as an additional Si wafer platform, to achieve such EF which makes the analysis more complicated. **Table 2** compiles SERS EF for different flexible substrates. Taken together, the simplicity of the fabrication strategy, high SERS EF, and pg/mL LOD make our plasmonic patch highly desirable for toxicology drug analysis.

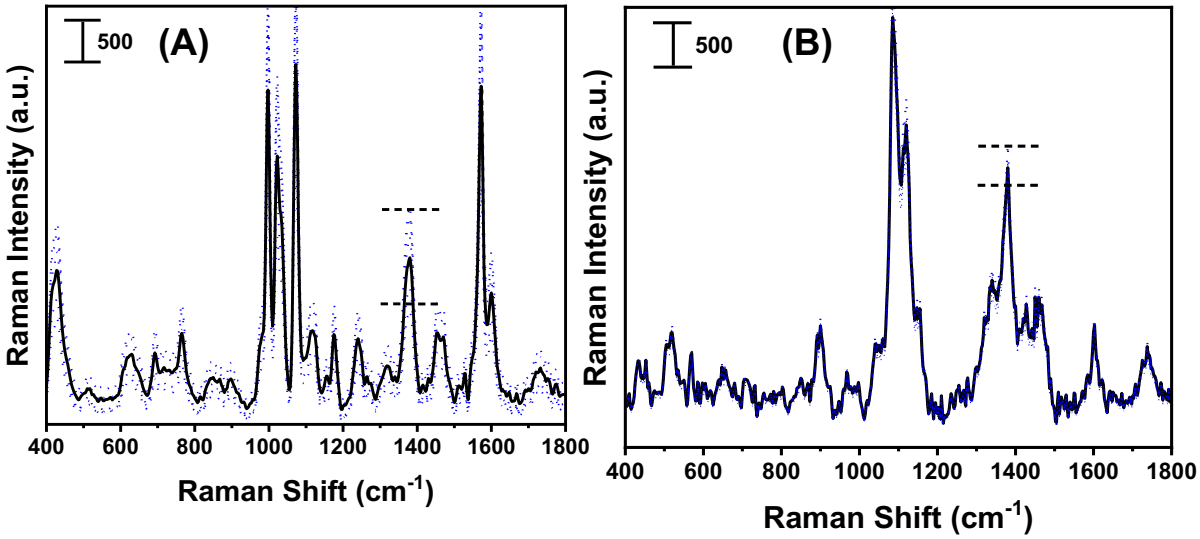

Figure 22. Representation of SERS spectra used to calculate S/N ratio of (A) TEA passivated Au TNPs adsorbed onto a flexible adhesive substrate (S/N = 4.8) and (B) the plasmonic patch (S/N = 12.5). S/N ratio was calculated by taking the mean of 1.0 nM fentanyl signal at 1384 cm^{-1} (black solid line) and dividing it by the standard deviation of the signal (black dashed lines). Mean was calculated from six measurements. All six measurements are represented by the blue dots. Adapted from Sardar et al. Anal. Chem. 2021.

We further tested the second hypothesis that the plasmonic patches should display low fouling effects compared to TEA-passivated Au TNPs adsorbed on either glass or flexible adhesive tape in the SERS analysis. A common analytical approach to determine the fouling effect is calculating signal-to-noise (S/N) ratios at the lowest analyte concentration.[27] The plasmonic patch displays a S/N value of 12.5 for fentanyl at 1.0 nM concentration. In contrast, TEA-passivated Au TNPs adsorbed onto a flexible adhesive substrate show a S/N value of 4.8 under identical experimental conditions. **Figure 22** shows SERS spectra used for S/N calculations. PEGs are commonly used to functionalize nanostructures in sensing applications because they reduce non-specific adsorption of endogenous biomolecules from biofluids.[39,41] Furthermore, the long glycol polymer should be able to wrap around TNPs, leaving no defect sites in the ligand layer where unwanted molecules could reach to the nanostructure surface. Under such conditions, analyte molecules

interact with PEG while endogenous biomolecules are repealled by PEGs. In contrast, TEA is a small molecule and would be unable to provide a homogeneous ligand packing leaving vacant sites, which allow molecular diffusion through them, leading to direct adsorption of analytes onto the TNP surface. Therefore, we believe that the lack of control over molecular diffusion in TEA-passivated Au TNPs causes adsorption of both fentanyl and plasma proteins on their surface, causing a higher fouling effect than PEG60-S-functionalized TNPs (plasmonic patch), overall producing a lower S/N ratio. One would expect that a shorter PEG chain thiolate ligand would improve the SERS sensitivity due to the presence of the analyte molecules much closer to the surface of a TNP; however, a shorter PEG could increase the fouling effects. Therefore, it would be interesting to determine the optimum PEG-thiolate chain length for TNP surface passivation to increase the sensitivity without compromising the non-fouling effect. This is part of our ongoing investigation.

To examine the interaction of analytes with ligand functionalized TNP surface in the SERS experiments, we further calculated the adsorption constant (K_{ad}) to quantitatively determine the affinity of such interaction. We used the Langmuir adsorption model to determine K_{ad} utilizing the SERS parameters for fentanyl as described below:[69,70]

$$I_s = \frac{I_{sm} K_{ad}[A]}{1 + K_{ad}[A]} \qquad (2)$$

Here, I_s and I_{sm} are the SERS intensity at the concentration A and at the saturation point of full monolayer coverage, respectively, and *[A]* is the concentration of adsorbate (fentanyl). The plotted data for plasmonic patches provide a K_{ad} value of 7.8 x 10^5 ± 2.4 L.mol^{-1} with an adjusted R^2 of 0.998 (**Figure 19C**). Interestingly, the K_{ad} value is 2.1 x 10^4 ± 1.3 L.mol^{-1} for TEA-passivated Au TNPs adsorbed onto a flexible adhesive tape. The result is significant and suggests that there is a relatively a strong interaction between PEG and fentanyl in comparison to fentanyl and TEA. Therefore, a stronger affinity of fentanyl towards plasmonic patches leads to the greater SERS signal enhancement, and thus the lower LOD and fouling effects.[69] Together, a relatively higher K_{ad} value for plasmonic patch is in agreement with our two hypotheses. The stability/shelf life of the plasmonic patch was also investigated by storing them under normal laboratory condition but covered with a protective layer to prevent prolonged light exposure. As shown in **Figure 23**, <3% relative standard deviation (RSD) is observed when fentanyl SERS spectra were collected every third day up to a month time.

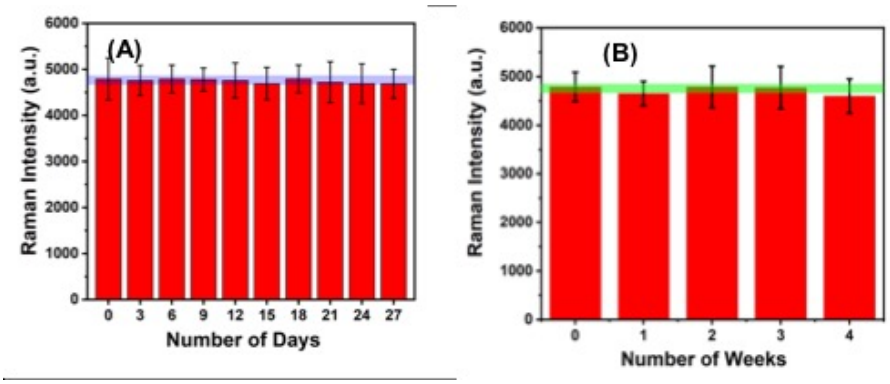

Figure 23. Stability Data. **(A)** An average Raman Intensity calculated from plasmonic patch when fentanyl SERS spectra was collected every third day for a month time. The transparent purple bar represents the obtained relative standard deviation, equal to < 3%. **(B)** An average Raman Intensity determined from plasmonic patch when fentanyl SERS spectra was collected every week for a month time. The transparent

green bar represents the obtained relative standard deviation, equal to 2.7%. Adapted from Sardar et al. Anal. Chem. 2021.

We further demonstrate that TDDFT calculations can be successfully implemented to support the unique interaction between the plasmonic patch and fentanyl discussed above. We performed TDDFT calculations of fentanyl in which its N atoms are forming hydrogen bonding with glycol units in aqueous medium. **Figure 19D** illustrates a comparison of experimental SERS spectrum (red curve) and TDDFT-calculated Raman spectrum (blue curve) of fentanyl. Clearly, H-C-N2 stretch at 1384 cm^{-1} and the aromatic C=C stretch at 1085 cm^{-1} of fentanyl perfectly match in experimental and theoretical spectra. Furthermore, the ratio of C=C to H-C-N2 stretch is almost the same for experimental and theoretical data. In contrast, this ratio is different for the TDDFT calculated fentanyl Raman spectrum (black curve) alone without any bonding interaction with the PEG in the plasmonic patch. Various vibrational modes of fentanyl for both experimental and TDDFT-calculated Raman spectra are provided in the Supporting Information (**Table 3**). Taken together, the above-mentioned experimental and theoretical results unequivocally prove that the plasmonic patch is the most suitable and efficient SERS substrate for drug detection in human plasma.

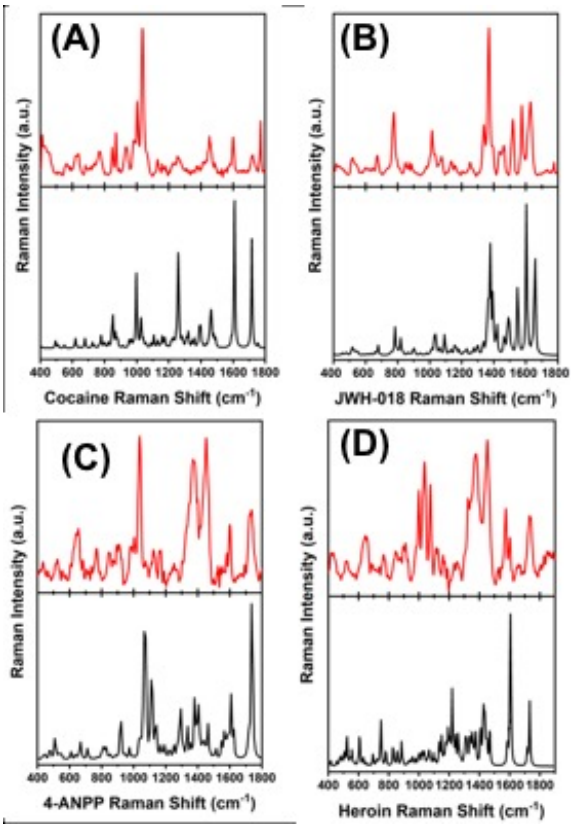

Figure 24. A comparison of experimentally acquired SERS spectrum (red curves) and theoretically calculated Raman spectra of glycol bound fentanyl (black curve) of (A) cocaine, (B) JWH-018, (C) 4-ANPP, and (D) heroin. The concentration of each drug is 1.0 nM. Adapted from Sardar et al. Anal. Chem. 2021.

5.2.2. Sensing Capabilities of the Plasmonic Patch for SERS-based Various Potent Drugs Analysis. An excellent SERS substrate should have the capability to detect any drug family such as coco alkaloids (cocaine), cannabinoids (JWH-018), and opioids (fentanyl, despropionyl fentanyl (4-ANPP), and heroin). Although, literature reports various SERS substrates for the detection of one or two types of drugs in human biofluids (saliva or urine) with high LODs (>ng/mL),[12,14,35,45,48,69] to the best of our knowledge, currently no SERS substrate exists that could be used to detect such a diverse range of potent drugs in human plasma at pg/mL concentrations. The generality of the plasmonic patch for SERS-based drug detection is further demonstrated for the above-mentioned drugs. 1.0 nM concentration drug solution was prepared in diluted human plasma and a total 6.0 μL was drop-casted onto the plasmonic patch. **Figure 24** shows experimentally acquired SERS spectra of cocaine, JWH-018, 4-ANPP, and heroin and the comparison with TDDFT-calculated Raman spectra of these drugs. Cocaine

displays characteristic aromatic stretch at 1253 and 1600 cm^{-1}, and C=O stretch at 1720 cm^{-1}.[14] All these vibrational modes are perfectly aligned with the theoretical calculations. Naphthalene C=C stretches of JWH-018 appear between 1300-1400 cm^{-1} along with C=O stretch at 1628 cm^{-1}. Another prominent peak of JWH-018 shows up at 775 cm^{-1} for indole ring stretch.[69] 4-ANPP shows all the characteristic aromatic peaks as similar to fentanyl. More specifically, a distinct N-H stretch is observed at 1035 cm^{-1} that is not present in fentanyl. The SERS spectrum of heroin is much more complicated than the other drugs. Importantly, we are able to determine C=O stretch at 1733 cm^{-1} and the entire O-C(=O)-C Raman stretch at 1233 cm^{-1}. SERS-based heroin detection has been reported in the literature[35,55] but a comprehensive list of the Raman stretch for different vibrational modes is still missing. Our thorough TDDFT calculations of heroin show a good match with the experimental spectra, and we are now able to assign most of the experimental Raman vibration modes (**Table 3-7**). Therefore, our calculated spectra could be the bedrock to the experimental scientists who are working on forensic science for illicit drug detection (seized drugs and forensic toxicology).

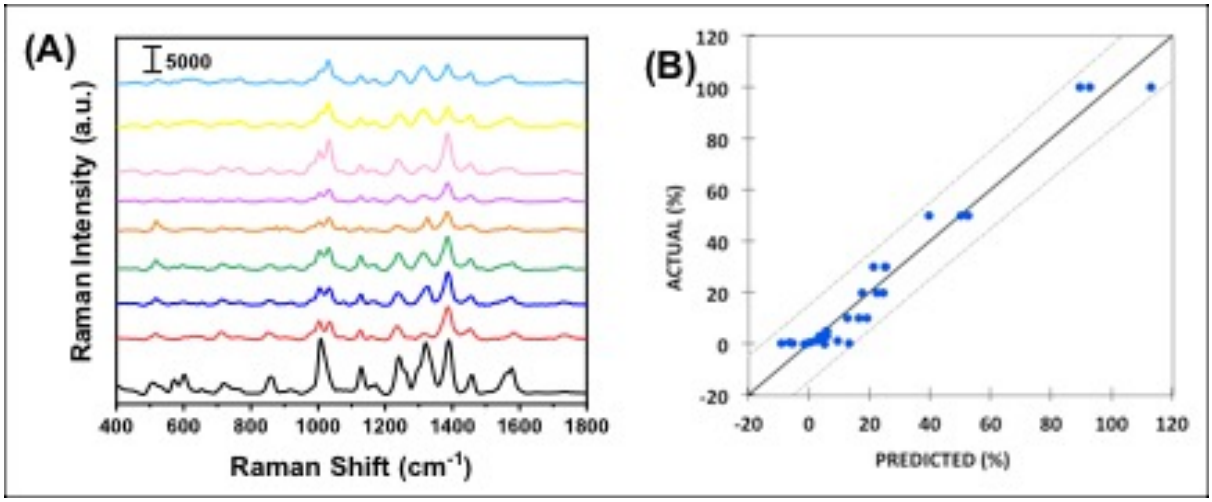

Figure 25. (A) SERS spectra of 0.15% to 50% fentanyl in heroin [Black = 50%, Red = 30%, Blue = 20%, Green = 10%, Orange = 5%, Light Purple = 3%, Pink = 1%, Yellow = 0.5%, Light Blue = 0.15%]. (B) Actual versus predicted concentrations based upon PCR. The solid line is the line of unity and the dashed lines represent the 95% confidence limits. The goodness of fit (R^2) was 0.96. Adapted from Sardar et al. Anal. Chem. 2021.

5.2.3. Specificity Test by Binary Mixture Analysis. Fentanyl is commonly used as an adulterant in heroin, and a few milligrams of fentanyl may cause an overdose due to its high potency. Therefore, precise quantification of trace quantity fentanyl in binary mixtures is of paramount importance to avoid drug related death and aid in the battle with opioid pandemic. Here we show that the plasmonic patches are capable of identifying fentanyl in binary mixture with heroin. Utilizing the SERS intensity ratio between isolated signature peaks for each drug (1384 cm^{-1} representing the H-C-N2 stretch for fentanyl and 1733 cm^{-1} representing the C=O vibration for heroin) we are able to identify 0.15 wt% fentanyl in heroin. As shown in **Figure 25A,** a wide range of weight percentages of fentanyl in heroin (0.15% to 50%) were analyzed utilizing SERS. As

shown in **Figure 25B**, heroin-to-fentanyl peak ratio is plotted, and the calibration curve is fitted to a Langmuir isotherm equation following the procedure reported by Haddad et al.[35] The calibration curve shows a linear increase in peak intensity ratio when the percentage of fentanyl in heroin increases (R^2=0.958), with a gradual plateau around 5% fentanyl in heroin. Importantly, the lethal concentrations of fentanyl found in binary mixtures are represented in the linear portion of the curve (mg of fentanyl in heroin), proving that the plasmonic patches are capable of detecting trace levels of fentanyl in binary mixtures. More importantly, this is the first example in which below 1 wt% fentanyl in heroin (as low as 0.15 wt%) can be detected utilizing our SERS substrates in comparison to the previous reported work by Haddad et al., where Ag NP-based SERS substrates were used.[35] In addition, we have also analyzed the SERS spectra obtained for each weight percentage through linear discriminant analysis. Principal component analysis (PCA) was used to generate a Scree Plot, which indicates that the first nine PCs are significant. These PCs represented 93.1% of the total variance in the data set. Replicates cluster well and subsequent discriminant analysis (DA) using the factor scores from the first nine PCs finds that the different concentrations could be discriminated with 90.9% accuracy **(Figure 26).** Lastly, principle component regression (PCR) generated a model with an R^2 of 0.96 and a root mean square error of 7.2. A plot of the actual versus predicted concentration values is shown in **Figure 25B**.

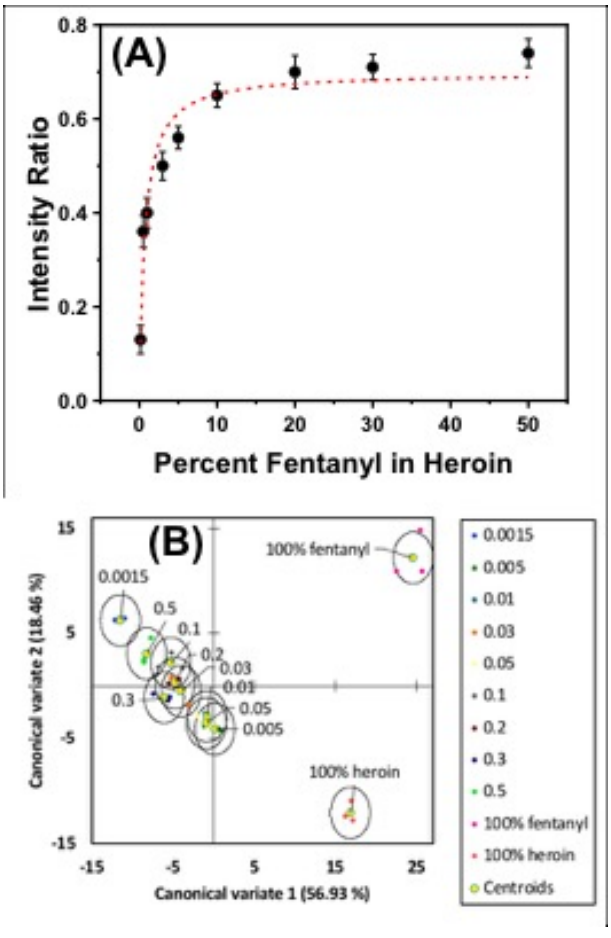

Figure 26. (A) Calibration curve using the peak intensity ratios of fentanyl (H-C-N2 Raman stretch at 1384 cm^{-1}) to heroin (-C=O Raman stretch at 1733 cm^{-1}) from 0.15-50%. Red dashed line represents calibration curve fitting using the Langmuir isotherm with R^2 = 0.959. (B) Scatter plot of the observations and class centroids plotted using the first two canonical variates as determined by discriminant analysis. The overall classification accuracy was 91%. Adapted from Sardar et al. Anal. Chem. 2021.

5.2.4. Application of the Plasmonic Patch in Forensic Toxicology. Since 1999, an average of 50,000 people die each year from opioid overdose.[71] Emergency department (ED) is the first line of defense to present death by performing initial diagnosis for DOA.[52] Opioids undergo fast decomposition in the metabolic system and their half-life is a few minutes to hours. Therefore, the concentration of undecomposed drugs in human biofluids is expected to be exceedingly low. This is a serious problem for the ED because currently used standard mass spectrometry and ELISA techniques for clinical diagnosis of drugs show low sensitivity. Therefore, there is an unmet need

for an ultrasensitive technique to identify drugs in the ED setting in order to find appropriate treatment and prevent death. We analyzed 10 patients' plasma samples, which were suspected to contain fentanyl, using the plasmonic patch for SERS-based detection. All the samples show characteristic fentanyl Raman stretch at 1384 cm^{-1} **(Figure 27A)**. Fentanyl concentration varies between 0.5-12 ng/mL. To further support SERS-based results, we performed PSI-MS analysis of these patient samples. We demonstrated the unique analytical capability of PSI-MS for toxicological drug screen in plasma of DOA patients without performing an extensive sample preparation.[72,73] As shown in **Figure 27B**, independently determined concentrations of 10 plasma samples are in excellent agreement between the two techniques. MS-MS spectra of 10 DOA samples showing fentanyl m/z values are provided in the supporting information **Figure 1-11**. **Table 8** provides concentration values determined by SERS and PSI-MS techniques for 10 DOA patient samples. Very recently, Driskell and coworkers reported combined SERS and PSI-MS techniques to analyze seized drugs; however, the method has not been applied to toxicological sample analysis.[66] As stated earlier, complexity of human biofluids increases fouling effects, and simple paper-based SERS substrate preparation is mostly unlikely to provide highly sensitive data. Nevertheless, we present the first example where spectroscopy and spectrometry techniques are used for toxicology drug analysis in real-world samples. We also conducted specificity tests of 10 patient plasma samples (DOA, n =10) with healthy individuals (normal control, NC, n=10) with a p-value of 0.0002 (**Figure 27C**). As illustrated in **Figure 27D**, receiving operating characteristic (ROC) analysis shows that the plasmonic patch-based SERS analysis of fentanyl is highly accurate to differentiate between DOA and NC with an area under the curve (AUC) is 0.97.

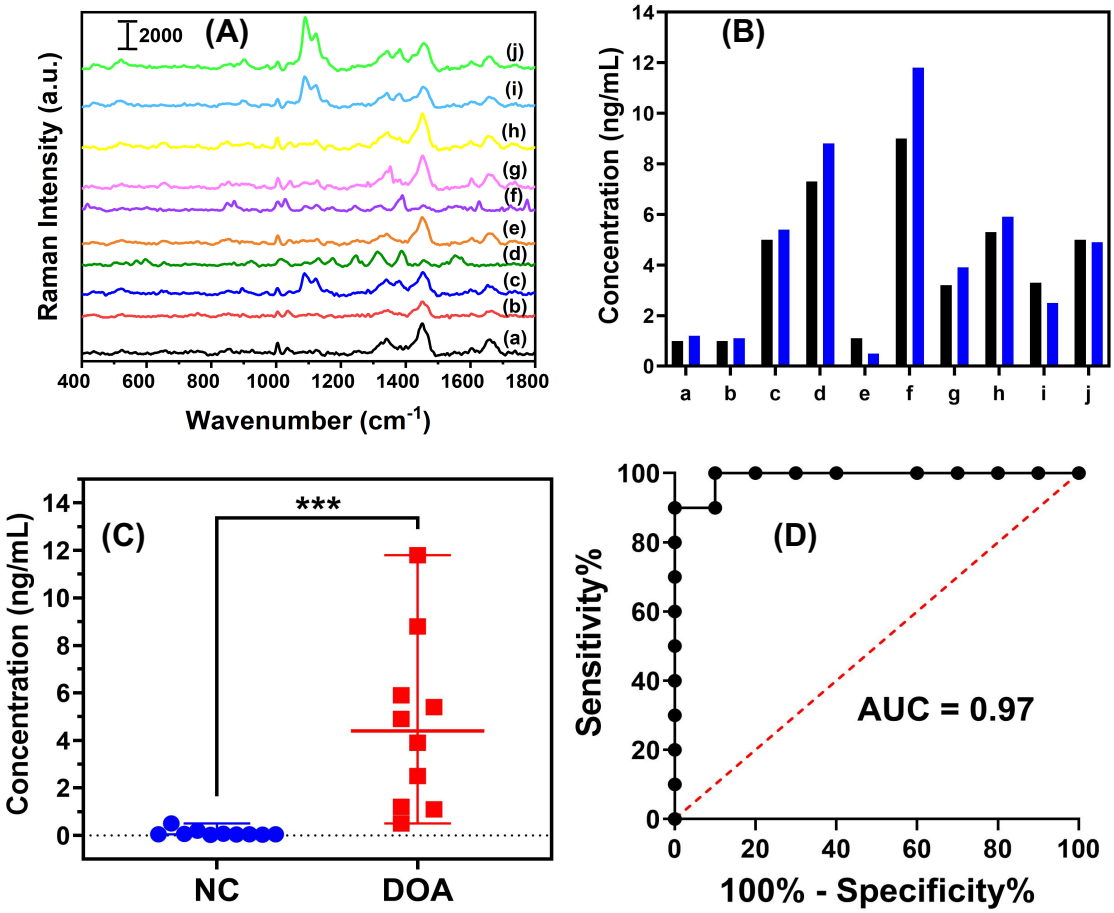

Figure 27. (A) SERS spectra of 6.0 μL-patient plasma diluted to 10% (v/v) with RNase free water and then drop-casted onto the plasmonic patch for the analysis. (B) The bar graph representing the concentration value of fentanyl in 10 patient samples where black and blue bars are respective concentrations determined by PSI-MS and SERS techniques. (C) Students t-test results of normal control verses drug-of-abuse (DOA) patient samples for fentanyl. (D) Receiver operating characteristic curve of normal control verses DOA patient samples. ***P< 0.0002 by t-test. Adapted from Sardar et al. Anal. Chem. 2021.

5.2.5. Summary. By fabricating a flexible and transparent plasmonic patch, we have demonstrated the highly sensitive, as low as 3.0 pg/mL, detection of potent drugs in human plasma by SERS technique. Moreover, the plasmonic patch mitigates fouling effects commonly caused by human biofluids. Plasmonic patch reported here shows higher SERS EF value (4.5 X 10^7) compared to the SERS substrate containing PEG60-thilate functionalized Au TNPs adsorbed onto non-flexible glass. Moreover, we have conducted drug adsorption behavior either on PEG60-S- or TEA-passivated Au TNPs adsorbed onto flexible SERS substrates that follows a Langmuir adsorption model, and the drug molecules shows a higher affinity towards PEG surface than TEA. We have successfully detected a range of potent drugs such as cocaine, JWH-018, fentanyl, despropionyl fentanyl, and heroin at 1.0 nM concentrations using the plasmonic patch. The experimental spectra are in good agreement with the TDDFT-calculated spectra and the results

suggest molecular level interactions between PEG and drug molecules. Most importantly, through chemometric analysis, we have shown excellent selectivity when mixtures of fentanyl in heroin were analyzed using the SERS technique. Using the SERS-based plasmonic patch, we have successfully characterized fentanyl in DOA patients' plasma and the concentration values are in excellent agreement with paper spray ionization-mass spectrometry results determined independently. Finally, ROC analysis presents excellent specificity of identifying fentanyl in DOA comparison to NC samples. Taken together, we believe that the excellent sensitivity and specificity of the plasmonic patch in SERS-based drug detection should be highly advantageous to clinical toxicology because low concentration of undecomposed drugs can be identified. We expect that the developed SERS substrate can also be used in therapeutic drug monitoring and post-mortem toxicology that together will dramatically simplify the *"war against drugs."*

6. Implication and Applicability to Criminal Justice

There are several implications to increasing the sensitivity, selectivity, specificity, and reproducibility of the instrumental/sensing methods applied to identify controlled substances.

(1) Improved **selectivity** allows for highly complex samples to be analyzed without extensive preliminary sample prep. Selective methods can determine the presence of an analyte even in the presence of interferences or metabolites thus eliminating false-positive results.

(2) Increased **specificity** removes doubts of the identification of a compound and increases the probative value of a determination. Drug analysis is impacted as criminal charges for consumption of a controlled substance can depend upon identifying a specific structural isomer of a specific chemical compound. Identification of isomers not demonstrated.

(3) Enhanced **reproducibility** provides precision in measurements regardless of who or where it is performed by following comparable procedures.

The development of ultrasensitive and highly specific SERS nanosensors has the potential to be an advanced analytical tool for forensic toxicology that creates a simple, cost effective and easily accessible means of analyzing human biofluids. Furthermore, enhanced drug detection sensitivity will decrease the likelihood of false negatives, which may be a barrier to criminal charging. Specifically, postmortem toxicology is one of the potential avenues where our technology can be successfully implemented to avoid the very high risk of matrix effects. Finally, and most importantly, the ultrasensitive nature of our SERS nanosensors should allow drug detection using a portable Raman instrument, thus will increase the scope of drug screening for forensic toxicologists, healthcare professionals, and law enforcement agencies for rapidly generating presumptive results by screening illegal drug consumption and overdose. Taken together, we believe that our tool will aid the forensic, healthcare, and law enforcement communities in the battle against the drug overdose epidemic in the United States.

➢ PRODUCTS

List of all Scholarly Products

1. Peer-Reviewed Publications: During the grant period, the following two peer-reviewed articles (number 1 and 2) have been published that are directly related to forensic toxicology.

Furthermore, we published several other articles (number 3-6), where Raman characterizations were conducted by using the instrument, which was purchased through NIJ support.

1. Liyanage, T.; Masterson, A. N.; Hati, S.; Ren, G. J.; Manicke, N.; Rusyniak, D.; **Sardar, R.** Optimization of electromagnetic hot spots in surface-enhanced Raman scattering substrates for an ultrasensitive drug assay of emergency department patients' plasma. *Analyst*, **2020**, *145*, 7662-7672.

2. Masterson, A. N.; Hati, S.; Ren, G. J.; Liyanage, T.; Manicke, N.; Goodpaster, J. V.; **Sardar, R.** Enhancing non-fouling and sensitivity of surface-enhanced Raman scattering substrates for potent drug analysis in blood plasma via fabrication of flexible plasmonic patch. *Anal. Chem*. **2021**. *93*, 2578-2588.

3. Lee, J. T.; Hati, S.; Fahey, M.; Zaleski, J.; **Sardar, R.** Surface ligand control enhancement of carrier density in plasmonic tungsten oxide nanocrystals: Spectroscopic observation of trap-state passivation via multidentate metal-phosphonate bonding. *Chem. Mater.* **2022**, *34*, 3053-3066.

4. Lee, J. T.; Wyatt, B. C.; Davis, G. A.; Masterson, A. N.; Pagan, A. L.; Shah, A.; Anasori, B.; **Sardar, R.** Covalent surface modification of Ti3C2Tx MXene with chemically active polymeric ligands producing highly conductive and ordered microstructure films. *ACS Nano* **2021**, *15*, 19600-19612.

5. Davis, G. A.; Prusty, G.; Hati, S.; Lee, J. T.; Langlais, S. R.; Zhan, X., **Sardar, R.** Design of Anisotropically-Shaped Plasmonic Nanocrystals from Ultrasmall Sn-Decorated In2O3 Nanoclusters Used as Seed Materials. *J. Phys. Chem. C* **2022**, 126, 21438-21452.

6. Lee, J. T.; Das, D.; Davis, G. A.; Hati, S.; Ramana, C.V.; **Sardar, R.** Inorganic-organic interfacial electronic effects in ligand-passivated WO3-x nanoplatelets induce tunable plasmonic properties for smart windows. *ACS Appl. Nano Mater.* **2022**, *5*, 9970-9980.

2. Thesis:

1. M. Vitoria Simas, M. S. Design and fabrication of smart SERS substrates for forensic science applications. June 2023.

2. Adrianna Masterson, Ph.D. Fabrication of LSPR-based multiplexed and high-throughput biosensor platforms for cancer and SARS-Cov-2 diagnosis. May 2022.

3. Thakshila Liyanage, Ph.D. Nanoplasmonic efficacy of gold triangular nanoprisms in measurement science: Applications ranging from biomedical to forensic science, December 2019.

List of all Dissemination Activities

1. Conference Presentations: During the grant period, the following oral and poster presentations were delivered in various international conferences. "Underline" signifies the presenter.

1. **Sardar, R.** Surface-enhanced Raman spectroscopy-based high-throughput toxicology drug screening. Pittcon Conference, Virtual meeting. March 2021. Oral presentation.

2. **Sardar, R.** Simplifying potent drug analysis in forensic toxicology by a surface-enhanced Raman spectroscopy-based, label-free technique. Pittcon Conference, Chicago, IL. March 2020, oral presentation.

3. Simas, V.; Manicke, N.; **Sardar, R**. Ultrasensitive Detection of Synthetic Drugs in Blood Plasma Using Hydrophobic Polymer-Modified Microneedle SERS Substrates. Pittcon Conference and Exposition, Philadelphia, Pennsylvania. March 18-22, 2023. Oral Presentation.

4. Simas, V.; Davis, G.; Hati, S.; **Sardar, R**. Shape-Dependent SERS Enhancement of Plasmonic WO_{3-x} Nanocrystals. Pittcon Conference and Exposition, Philadelphia, Pennsylvania. March 18-22, 2023. Poster Presentation.

5. Simas, V.; Manicke, N.; **Sardar, R**. Drug detection using a tip-enhanced Raman spectroscopy analogous plasmonic sharp tip substrate. ACS Spring 2023: Crossroads of Chemistry, Indianapolis, Indiana. March 26-30, 2023. Poster Presentation.

6. Simas, V.; Davis, G.; Hati, S.; **Sardar, R**. Morphology dependent SERS enhancement of plasmonic WO_{3-x} nanostructures. ACS Spring 2023: Crossroads of Chemistry, Indianapolis, Indiana. March 26-30, 2023. Oral Presentation.

7. Simas, V.; Manicke, N.; **Sardar, R**. Combining Surface-Enhanced Raman Spectroscopy (SERS) and Mass Spectrometry Techniques to Increase Sensitivity and Specificity in Toxicological Drug Analysis in Blood Plasma. 2023 NIJ Forensic Science R&D Symposium, Orlando, Florida. February 14th, 2023. Poster Presentation.

8. Masterson, A. N.; Hati, S.; Ren, G.; Liyanage, T.; Manicke, N. E.; Goodpaster, J. V.; **Sardar, R**. Optimizing structural parameters of SERS substrates for highly specific and sensitive toxicological drug assays. ACS national meeting Atlanta, Georgia. August 22-26, 2021. Oral presentation.

9. Masterson, A. N.; Liyanage, T.; Albarbari, N.; **Sardar, R**. Development of an Ultrasensitive Sensor for Toxicology Screening of Undecomposed Drugs using a Portable Raman Instrument. Pittcon Conference, Chicago, IL. March 2020. NIJ poster presentation.

10. Liyanage, T.; Sardar, R. Evaporative self-assembly of gold nanoprisms for the ultrasensitive SERS-based drug careening from patient plasma. Pittcon conference, Philadelphia, PA. March 2019, oral presentation.

➢ Supporting Information

Table 1. Density Functional theory-based Raman stretches of fentanyl, cocaine, and JWH-018. All the vibrational modes are assigned as reported in the literature.[10-12]

Vibrational Description	Only Fentanyl		Fentanyl-Glycol		Fentanyl-Au		Experimental
	Mode	DFT/cm^{-1}	Mode	DFT/cm^{-1}	Mode	DFT/cm^{-1}	SERS/cm^{-1}
ν (C═C)$_{B1}$	124	1,642	172	1,642	127	1,580	1,573
δ (CH$_2$)$_{pip}$	118	1,506	161	1,498	121	1,476	1,469
δ (H-C-N2)	103	1,390	142	1,399	107	1,372	1,338
ν (N1-C-C-C)$_{B1}$; γ$_t$ (CH$_2$)$_β$	85	1,222	119	1,219	82	1,140	1,106
δ (CH)$_{B1,B2}$	76	1,124	106	1,102	76	1,068	1,079
ν (C═C)$_{B1,B2}$; δ (CH)$_{B1,B2}$	70	1,052	96	1,048	71	1,004	1,002
δ (C═C)$_{B2}$; ν (C$_ε$-C$_1$-C$_2$)	65	1,017	90	1,021	64	972	962
δ$_r$ (CH$_2$)$_{pip}$; ν (C$_ε$-C$_1$-C$_2$)	57	966	83	976	59	916	937
ν (C$_{B1}$-C$_α$-C$_β$-N$_1$); β (ring)$_{B1}$	45	778	64	751	52	820	852
γ$_t$ (CH$_3$); δ$_r$ (CH$_2$)$_{pip}$; δ (C$_ε$-C$_1$-C$_2$)	42	754	63	724	46	724	725
δ (ring)$_{B1,B2}$; δ$_r$ (CH$_2$)$_{alkyl}$; δ$_r$ (CH$_3$)	37	636	57	634	42	628	628

ν = stretching, δ = in plane deformation (*sc* = scissoring, *r* = rocking), γ = out of plane deformation (w = wagging, t = twisting), β = breathing.

Vibrational Descriptions	Cocaine-Au		Experimental
	Mode	DFT/cm^{-1}	SERS/cm^{-1}
υ (C=O, benzoate ester)	104	1,604	1,574
δ (benzene ring)	90	1,380	1,390
ω (CH, piperidine ring) + ω$_s$(CH$_2$, piperidine ring)	88	1,356	1,315
ν$_{as}$ (HC−C−O) + δ (benzene ring) + ω (CH$_2$-CH, piperidine/pyrollidine ring)	79	1,236	1,228
ν (C−O, piperidine ester) + β$_{as}$ (C−H$_3$, piperidine ester) + γ (piperidine/pyrollidine ring) + ω (C−H, piperidine ester)	68	1,180	1,170
δ (benzene ring)	55	988	1,077
ν$_s$ (H$_2$C−CH−CH, piperidine ring) + ν$_{as}$ (H$_2$C−CH$_2$−CH$_2$, pyrollidine ring)	48	876	1,000
γ (piperidine/pyrollidine ring)	44	804	817
γ (benzene ring)	41	756	717
δ (benzene ring)	33	620	637

υ = stretching; δ = in-plane distortion; γ = out-of-plane distortion; ω = wagging; τ = torsion; β = breathing; s = symmetric; as = antisymmetric

Vibrational Descriptions	JWH-018-Au		Experimental
	Mode	DFT/cm^{-1}	SERS/cm^{-1}
v (C=O)	120	1,604	1,581
δ_{sc} (CH_2); δ_{sc} (CH_3); δ_{sc} (CH_2) I2; δ_{sc} (CH) Nph	116	1,492	1,459
δ_r (CH) Nph	104	1,420	1,392
v (C=C) Nph	100	1,388	1,312
γ_t (CH_2); δ_{sc} (CH) I2, N2	91	1,276	1,242
δ_{sc} (HC-CH) I2, N1	83	1,188	1,168
δ_{sc} (HC-CH) Nph	78	1,140	1,127
δ_{sc} (HC-C-CH) N1	74	1,060	1,076
β (ring) I2; v (C-C) tail	69	1,012	1,014
v (C-CH_3); δ (ring) I2, Nph	60	908	922
δ_r (CH_2); δ_r (CH_3); γ_w (CH)-N-CH	52	796	856
β (ring) Ind; γ_w (CH) Nph	49	764	775
δ (ring) Nph	41	668	713
δ (ring) I1, Nph	40	644	659
δ (ring) Ind, Nph	33	508	580
γ_w (CH) Nph; δ (ring) Ind	31	468	497

ν = stretching, δ = in plane deformation (*sc* = scissoring, *r* = rocking), γ = out of plane deformation (w = wagging, t = twisting), β = breathing. Nph = Naphthalene; Ind = Indole; N1 and N2 refer to the two rings in naphthalene. I1 and I2 refer to the two rings in indole.

Table 2. *Summarization of different obtained SERS-EF for flexible substrate found in the literature.*

SERS Substrate	Analyte	Ef	Reference
Silver nanoparticles on cotton swab	Rhodamine 6G	1.6×10^6	[74]
Silver nanoparticles on filter paper	Fentanyl	3.1×10^7	[75]
Gold nanorod clusters on SIS polymer film	Crystal violet	4.5×10^6	[76]
Gold nanoparticles on PMMA polymer film	Malachite green isothiocyanate	2.4×10^7	[77]
Gold and silica nanoparticles on PDMS polymer film	Benzenethiol	7.1×10^3	[78]
Silver nanoparticles on PDMS polymer film	Aminothiolphenol	4.6×10^6	[79]
Gold nanostars on PDMS polymer film on silicon wafer	Benzenethiol	1.9×10^8	[80]
Gold film on gel tape	Crystal violet	1.5×10^6	[81]
Silver nanocubes on adhesive tape	Aminothiophenol	3.2×10^6	[82]
Gold nanoparticles on adhesive tape	4-Mercaptopyridine	1.3×10^5	[83]
Gold triangular nanoprisms on adhesive tape	Fentanyl	4.5×10^7	Current work

Table 3. *Various vibrational modes of fentanyl for TDDFT-calculated Raman spectra and experimental SERS spectra. Scale factor for TDDFT spectra is 0.93.*

Vibrational Description	Fentanyl		Fentanyl-Glycol		Experimental
	Mode	DFT (cm^{-1})	Mode	DFT (cm^{-1})	SERS (cm^{-1})
ν (C═C)$_{B1}$	124	1,757	172	1,756	1,738
δ (CH$_2$)$_{pip}$	118	1,602	161	1,603	1,603
δ (H-C-N2)	103	1,402	142	1,381	1,384
ν (N1-C-C-C)$_{B1}$; γ_t (CH$_2$)$_\beta$	85	1,302	119	1,296	1,300
δ (CH)$_{B1,B2}$	76	1,202	106	1,227	1,252
ν (C═C)$_{B1,B2}$; δ (CH)$_{B1,B2}$	70	1,125	96	1,121	1,120
δ (C═C)$_{B2}$; ν (C$_\varepsilon$-C$_1$-C$_2$)	65	1,087	90	1,087	1,085
δ_r (CH$_2$)$_{pip}$; ν (C$_\varepsilon$-C$_1$-C$_2$)	57	1,033	83	986	997
ν (C$_{B1}$-C$_\alpha$-C$_\beta$-N$_1$); β (ring)$_{B1}$	45	979	64	919	900
γ_t (CH$_3$); δ_r (CH$_2$)$_{pip}$; δ (C$_\varepsilon$-C$_1$-C$_2$)	42	809	63	774	710
δ (ring)$_{B1,B2}$; δ_r (CH$_2$)$_{\alpha+B1}$; δ_r (CH$_3$)	37	679	57	678	659

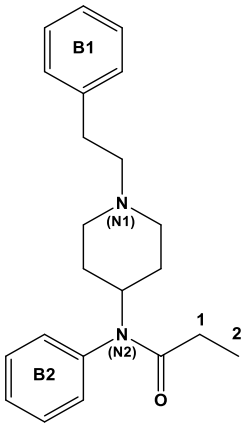

ν = stretching, δ = in plane deformation (*sc* = scissoring, *r* = rocking), γ = out of plane deformation (w = wagging, t = twisting), β = breathing
pip = piperidine ring

Table 4. *Various vibrational modes of cocaine for TDDFT-calculated Raman spectra and experimental SERS spectra. Scale factor for TDDFT is 0.98.*

Vibrational Description	Cocaine-Glycol		Experimental
	Mode	DFT (cm^{-1})	SERS (cm^{-1})
υ (C=O, benzoate ester)	125	1,717	1,720
δ (benzene ring)	124	1,609	1,600
ω (CH, piperidine ring) + ω (CH_2, piperidine ring)	115	1,462	1,453
ν (HC−C−O) + δ (benzene ring) + ω (CH_2-CH, piperidine/pyrollidine ring)	108	1,397	1,380
ν (C−O, piperidine ester) + β (C−H_3, piperidine ester) + γ (piperidine/pyrollidine ring) + ω (C−H, piperidine ester)	101	1,321	1,315
δ (benzene ring)	94	1,258	1,253
ν (H_2C−CH−CH, piperidine ring) + ν (H_2C−CH_2−CH_2, pyrollidine ring)	70	1,027	1,035
γ (piperidine/pyrollidine ring)	67	998	1,003
γ (benzene ring)	55	853	848
δ (benzene ring)	40	620	638

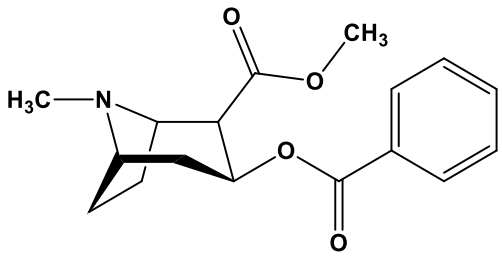

ν = stretching, δ = in plane deformation (*sc* = scissoring, *r* = rocking), γ = out of plane deformation (w = wagging, t = twisting), β = breathing

Table 5. *Various vibrational modes of JWH-018 for TDDFT-calculated Raman spectra and experimental SERS spectra. Scale factor for TDDFT is 0.0.*

Vibrational Description	JWH-018 -Glycol		Experimental
	Mode	DFT (cm^{-1})	SERS (cm^{-1})
v (C=O)	138	1,659	1,628
δ_{SC} (CH_2) N2	137	1,603	1,575
δ_{SC} (CH_2); δ_{SC} (CH_3); δ_{SC} (CH_2) I2; δ_{SC} (CH) Nph	136	1,547	1,520
δ_r (CH) Nph	119	1,491	1,463
v (C=C) Nph	114	1,379	1,370
γ_t (CH_2); δ_{SC} (CH) I2, N2	104	1,295	1,253
δ_{SC} (HC-CH) I2, N1	99	1,232	1,205
δ_{SC} (HC-CH) Nph	91	1,155	1,138
δ_{SC} (HC-C-CH) N1	86	1,092	1,075
β (ring) I2; v (C-C) tail	76	1,036	1,015
v (C-CH_3); δ (ring) I2, Nph	68	903	890
δ_r (CH_2); δ_r (CH_3); γ_w (CH)-N-CH	60	819	800
β (ring) Ind; γ_w (CH) Nph	57	784	775
δ (ring) Nph	49	679	673
δ (ring) Ind, Nph	39	518	518

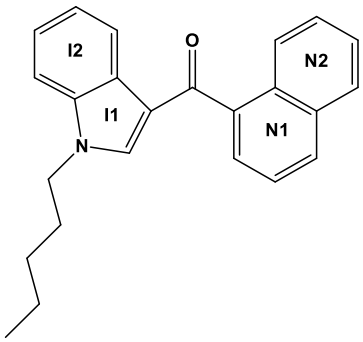

v = stretching, *δ* = in plane deformation (*sc* = scissoring, *r* = rocking), *γ* = out of plane deformation (w = wagging, t = twisting), β = breathing

Nph = Naphthalene; Ind = Indole
N1 and N2 refer to the two rings in naphthalene
I1 and I2 refer to the two rings in indole

Table 6. *Various vibrational modes of 4-ANPP for TDDFT-calculated Raman spectra and experimental SERS spectra. Scale factor for TDDFT is 1.05.* Adapted from Sardar et al. Anal. Chem. 2021.

Vibrational Description	4-ANPP -Glycol		Experimental
	Mode	DFT (cm^{-1})	SERS (cm^{-1})
$\nu\ (C{=}C)_{B2}$	152	1,735	1,735
$\delta_{sc}\ (CH_2)_{pip}$	144	1,608	1,600
$\nu\ (C_\eta\text{-}N_1)$; $\beta\ (CH)_{pip}$	126	1,566	1,528
$\nu_{sm}\ (CH_2)_{pip}$; $\delta_r\ (CH)_{B1}$	118	1,405	1,453
$\nu_{asm}\ (CH_2)_{pip}$; $\delta_r\ (CH)_{B2}$	114	1,380	1,373
$\nu\ (C_\alpha\text{-}C_\eta)_{\alpha+B1}$	107	1,295	1,253
$\nu\ (C{=}C)_{B2}$; $\delta_{sc}\ (CH)_{B1}$	89	1,143	1,170
$\nu\ (C{=}C)_{B1}$; $\delta_{sc}\ (CH)_{B2}$	84	1,109	1,075
$\delta_{sc}\ (C{=}C)_{B2}$	79	1,066	1,038
$\delta_r\ (CH_2)_{\alpha+B1}$	73	1,024	1,005
$\nu\ (C\text{-}N_2\text{-}C)$	66	916	910
$\delta_r\ (CH_2)_{pip}$; $\gamma_t\ (CH)_{B1}$	57	809	845
$\delta_r\ (C{=}C)_{B1}$; $\delta_{sc}\ (CH_2)_{\alpha+B1}$	50	664	655
$\gamma_w\ (CH)_{B1}$	41	504	523

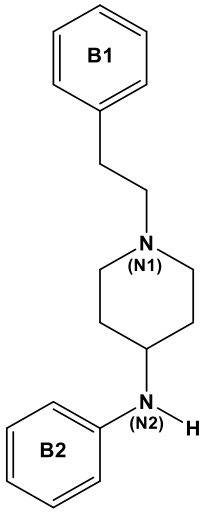

ν = stretching, δ = in plane deformation (*sc* = scissoring, *r* = rocking), γ = out of plane deformation (w = wagging, t = twisting), β = breathing

pip = piperidine ring

Table 7. *Various vibrational modes of heroin for TDDFT-calculated Raman spectra and experimental SERS spectra. Scale factor for TDDFT is 0.81.* Adapted from Sardar et al. Anal. Chem. 2021.

Vibrational Description	Heroin-Glycol		Experimental
	Mode	DFT (cm^{-1})	SERS (cm^{-1})
ν (C═O)	142	1,733	1,733
$\nu (C{=}C)_C$	139	1,606	1,575
$\nu (C{=}C)_A$, $\delta_{SC} (CH_2)_B$	126	1,428	1,453
$\delta_{SC} (CH)_C$	119	1,378	1,378
$\delta_r (CH_2)_D$	101	1,312	1,325
$\delta_r (CH)_A$, $\delta_r (CH_2)_B$	92	1,220	1,253
δ_{SC} (CH-CH)$_B$, ν (O-C(=O)-C) Tail	89	1,193	1,233
$\nu (C{=}C)_C$, $\delta_{SC}(CH_2)_D$	84	1,150	1,188
$\nu (C{=}C)_A$, $\nu (N\text{-}CH_3)_D$	82	1,135	1,160
$\nu (C\text{-}C)_B$	80	1,096	1,113
γ_t (C-C-C)$_C$	79	1,066	1,075
$\gamma_w (CH_3)$ Tail	77	1,035	1,038
$\delta_{SC} (CH)_A$	74	1,004	1,000
γ_w (C-C)$_A$	67	884	910
γ_w (C-C)$_C$	64	857	875
γ_w (C-C)$_B$	63	826	847
$\delta_r (C\text{-}C)_C$	58	749	768
γ_t (Ring A)	50	606	648
$\beta(C\text{-}H)_{AC}$	41	525	518

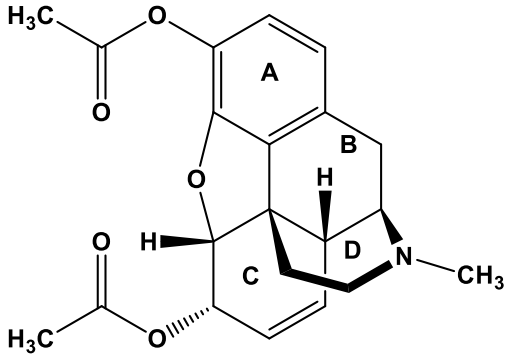

ν = stretching, δ = in plane deformation (*sc* = scissoring, *r* = rocking), γ = out of plane deformation (w = wagging, t = twisting), β = breathing

Table 8. *Calculated fentanyl concentrations in DOA patient samples determined by SERS and PSI-MS.* Adapted from Sardar et al. Anal. Chem. 2021.

Patient no.	Paper Spray MS Conc. (ng/mL)	SERS Plasmonic Patch Conc. (ng/mL)
(a)	1.0	1.2
(b)	1.0	1.1
(c)	5.0	5.4
(d)	7.3	8.8
(e)	1.1	0.5
(f)	9.0	11.8
(g)	3.2	3.9
(h)	5.3	5.9
(i)	3.3	2.5
(j)	5.0	4.9

- **Supporting Information Figures (**All these figures are adapted from Sardar et al. Anal. Chem. 2021).

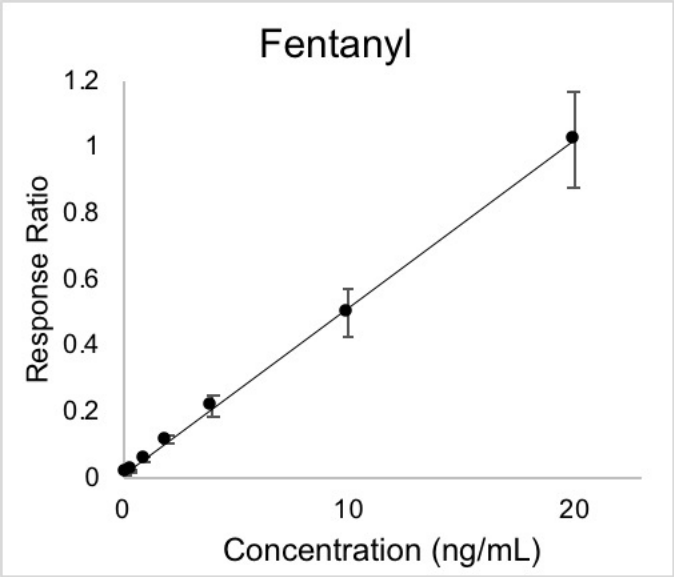

Figure 1. *Calibration curve for fentanyl in pooled human donor plasma for PS-MS analysis.*

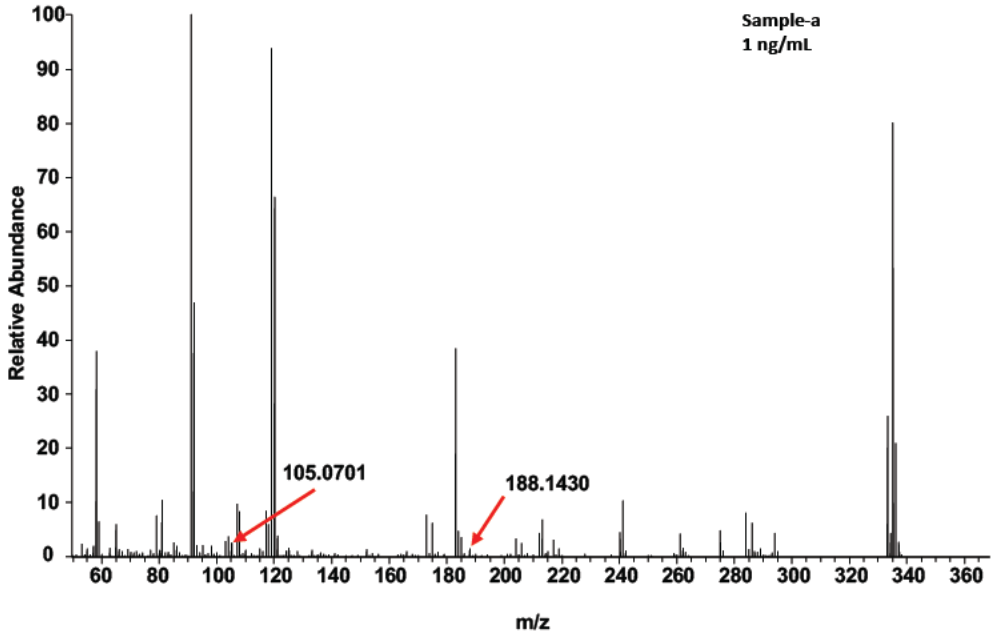

Figure 2. *MS/MS spectra of DOA patient plasma-a. The m/z peak at 337 is for intact fentanyl and the fragments are appeared m/z at 105 and 108.*

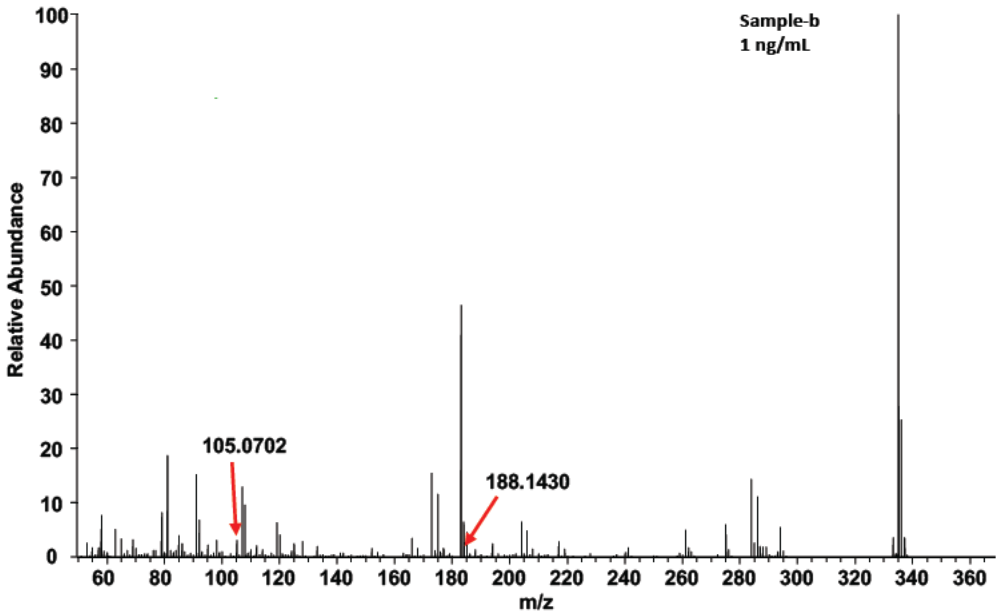

Figure 3. *MS/MS spectra of DOA patient plasma-b. The m/z peak at 337 is for intact fentanyl and the fragments are appeared m/z at 105 and 108.*

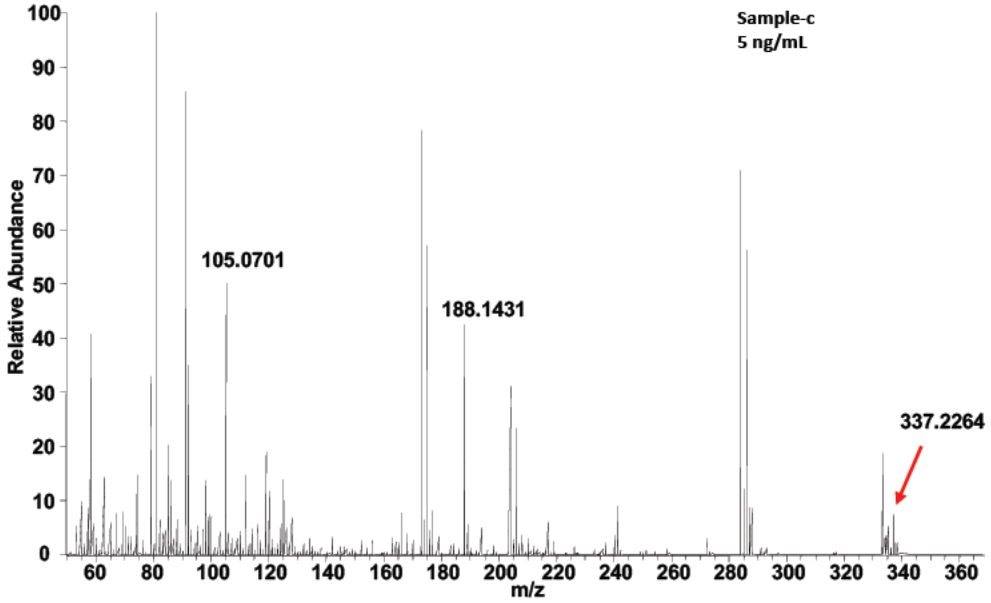

Figure 4. *MS/MS spectra of DOA patient plasma-c. The m/z peak at 337 is for intact fentanyl and the fragments are appeared m/z at 105 and 108.*

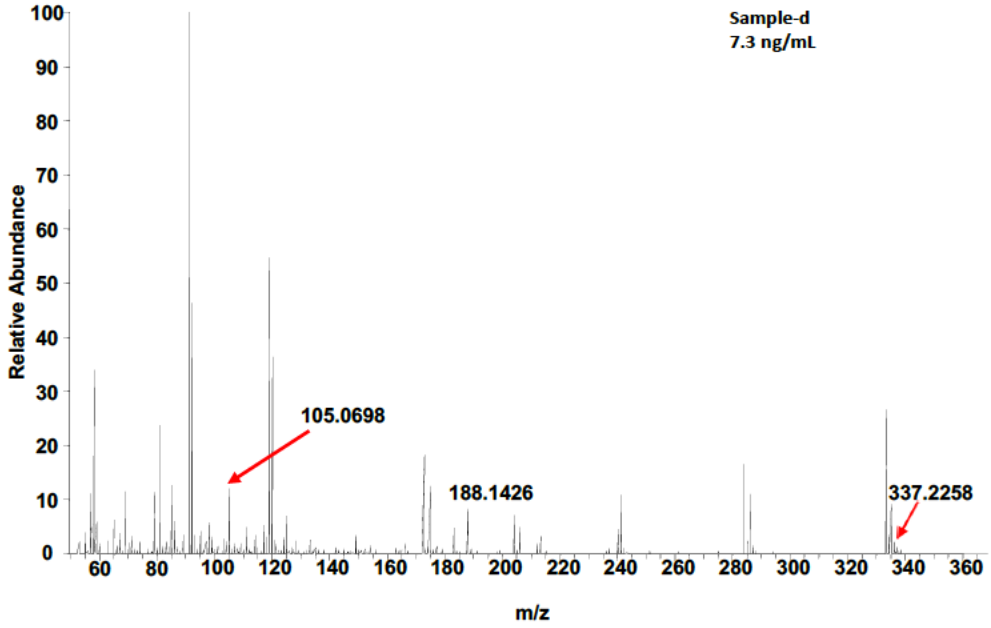

Figure 5. *MS/MS spectra of DOA patient plasma-d. The m/z peak at 337 is for intact fentanyl and the fragments are appeared m/z at 105 and 108.*

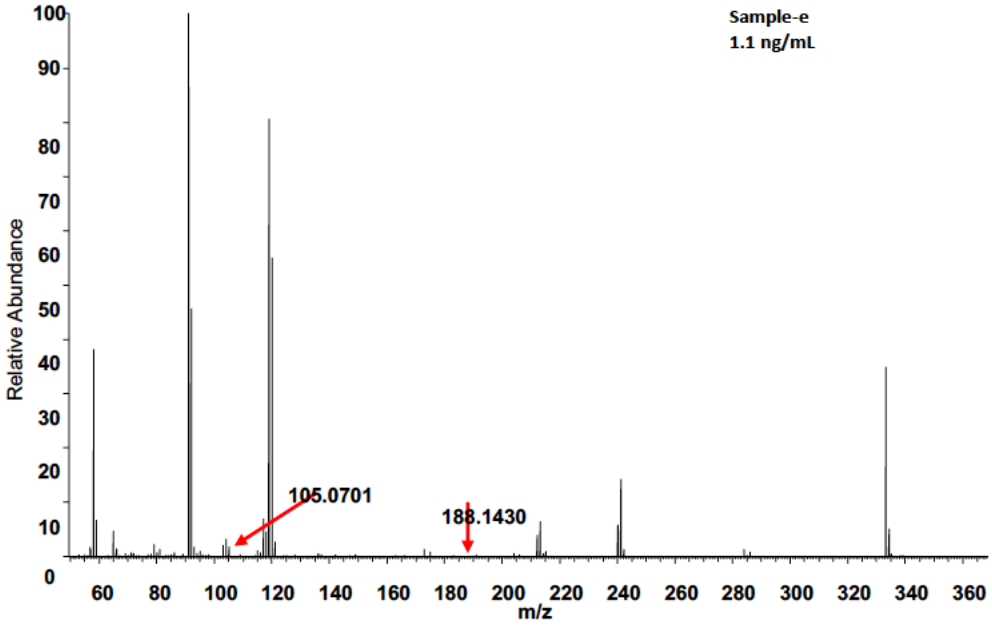

Figure 6. *MS/MS spectra of DOA patient plasma-e. The m/z peak at 337 is for intact fentanyl and the fragments are appeared m/z at 105 and 108.*

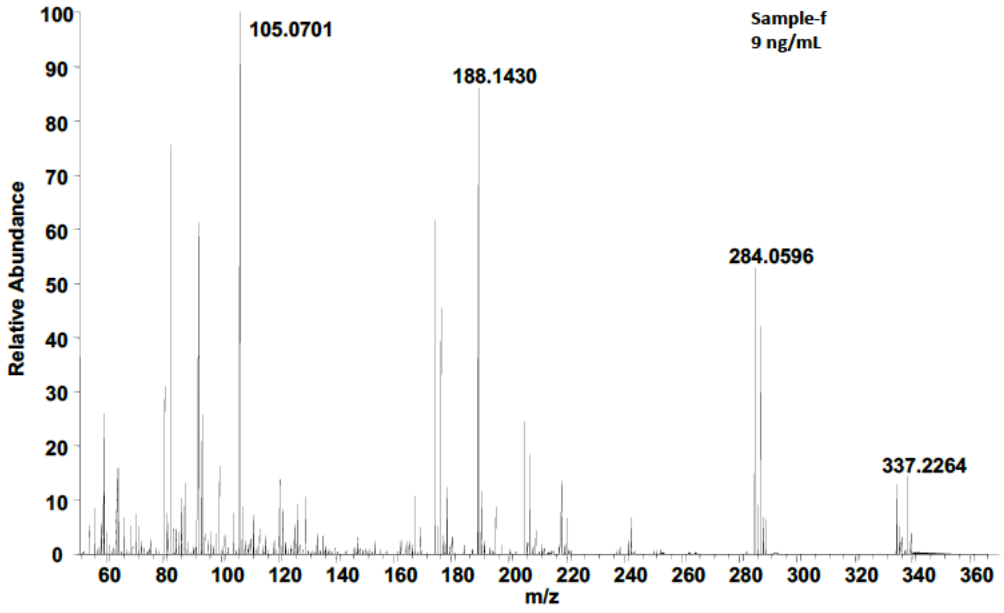

Figure 7. *MS/MS spectra of DOA patient plasma-f. The m/z peak at 337 is for intact fentanyl and the fragments are appeared m/z at 105 and 108.*

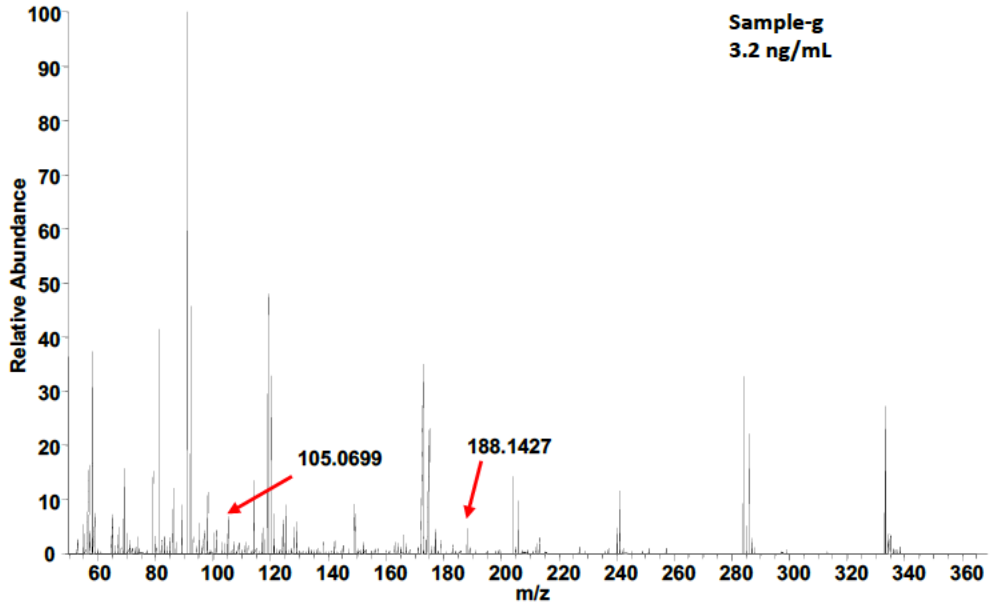

Figure 8. *MS/MS spectra of DOA patient plasma-g. The m/z peak at 337 is for intact fentanyl and the fragments are appeared m/z at 105 and 108.*

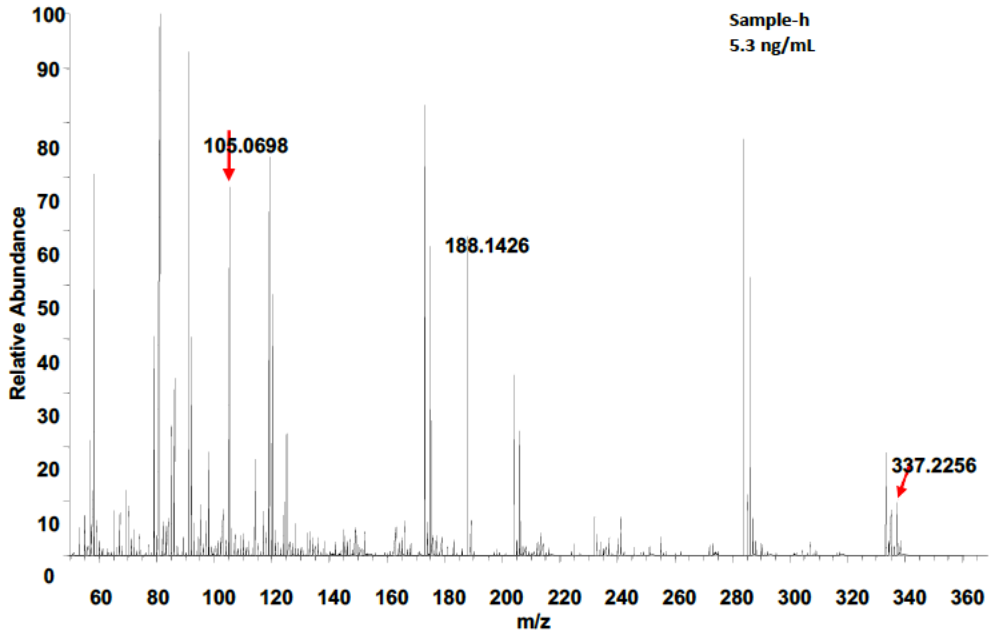

Figure 9. *MS/MS spectra of DOA patient plasma-h. The m/z peak at 337 is for intact fentanyl and the fragments are appeared m/z at 105 and 108.*

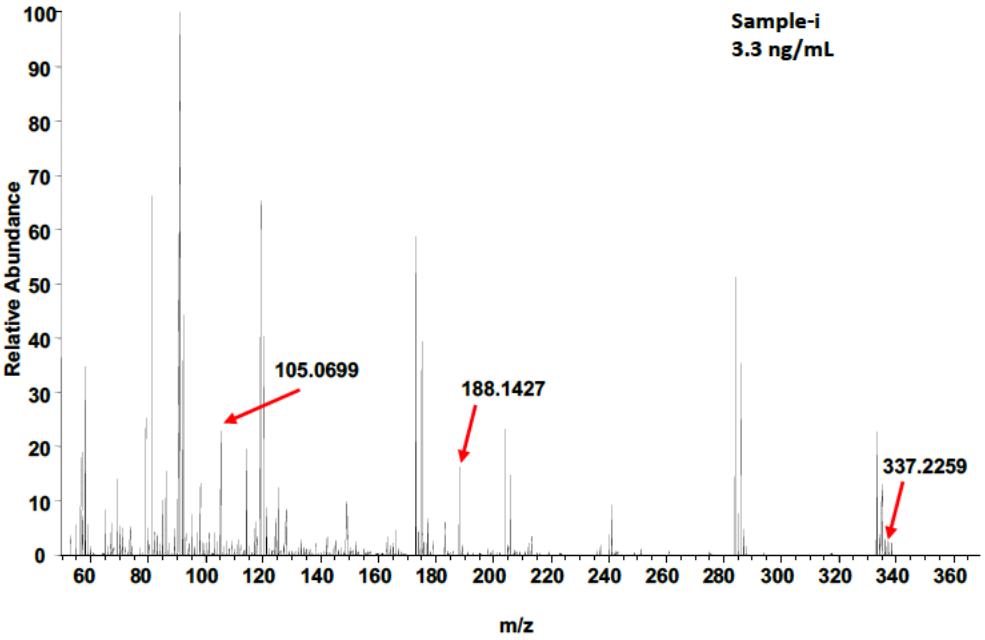

Figure 10. *MS/MS spectra of DOA patient plasma-i. The m/z peak at 337 is for intact fentanyl and the fragments are appeared m/z at 105 and 108.*

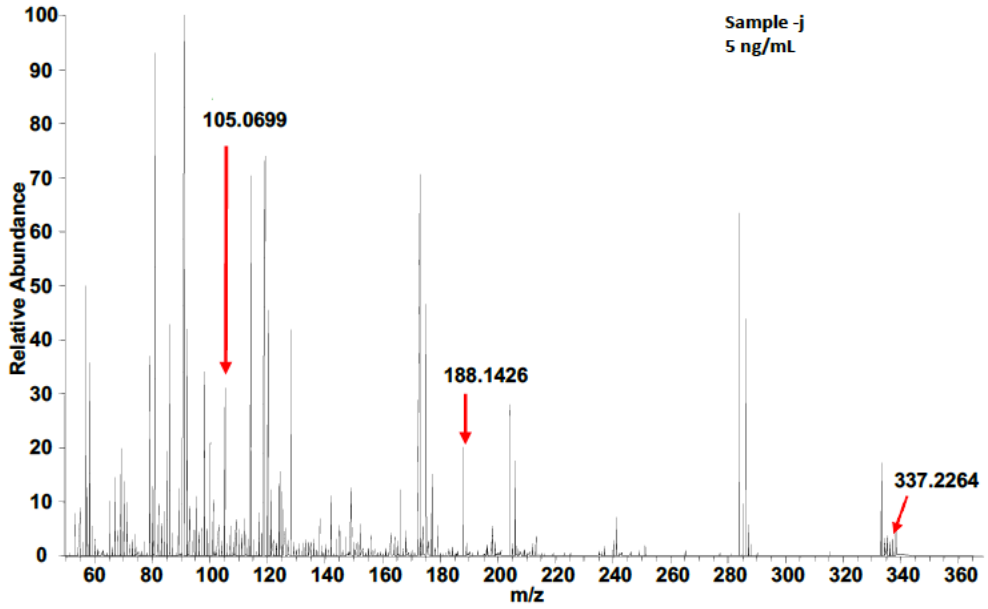

Figure 11. *MS/MS spectra of DOA patient plasma-j. The m/z peak at 337 is for intact fentanyl and the fragments are appeared m/z at 105 and 108.*

➢ REFERENCES

1 Saber Tehrani, M., Givianrad, M. H. & Mahoor, N. Surfactant-assisted dispersive liquid-liquid microextraction followed by high-performance liquid chromatography for determination of amphetamine and methamphetamine in urine samples. *Anal. Method.* **4**, 1357-1364 (2012). https://doi.org:10.1039/C2AY25125F

2 Strano-Rossi, S., Colamonici, C. & Botrè, F. Parallel analysis of stimulants in saliva and urine by gas chromatography/mass spectrometry: Perspectives for "in competition" anti-doping analysis. *Analytica Chimica Acta* **606**, 217-222 (2008). https://doi.org:http://dx.doi.org/10.1016/j.aca.2007.10.053

3 Welter, J., Meyer, M. R., Kavanagh, P. & Maurer, H. H. Studies on the metabolism and the detectability of 4-methyl-amphetamine and its isomers 2-methyl-amphetamine and 3-methyl-amphetamine in rat urine using GC-MS and LC-(high-resolution)-MS n. *Analytical and Bioanalytical Chemistry* **406**, 1957-1974 (2014). https://doi.org:10.1007/s00216-013-7595-5

4 Pujol, M.-L., Cirimele, V., Tritsch, P. J., Villain, M. & Kintz, P. Evaluation of the IDS One-Step™ ELISA kits for the detection of illicit drugs in hair. *Forensic Science International* **170**, 189-192 (2007). https://doi.org:http://dx.doi.org/10.1016/j.forsciint.2007.02.032

5 Han, E. *et al.* Validation of the Immunalysis® Microplate ELISA for the Detection of Methamphetamine in Hair. *J. Anal. Toxico.* **30**, 380-385 (2006). https://doi.org:10.1093/jat/30.6.380

6 Djozan, D., Farajzadeh, M. A., Sorouraddin, S. M. & Baheri, T. Molecularly imprinted-solid phase extraction combined with simultaneous derivatization and dispersive liquid–liquid microextraction for selective extraction and preconcentration of methamphetamine and ecstasy from urine samples followed by gas chromatography. *Journal of Chromatography A* **1248**, 24-31 (2012). https://doi.org:http://dx.doi.org/10.1016/j.chroma.2012.05.085

7 Gaillard, Y. P. *et al.* A Fatality Following Ingestion of the Designer Drug Meta-Chlorophenylpiperazine (mCPP) in an Asthmatic—HPLC-MS/MS Detection in Biofluids and Hair. *Journal of Forensic Sciences* **58**, 263-269 (2013). https://doi.org:10.1111/j.1556-4029.2012.02254.x

8 Scientific Working Group for Forensic Toxicology (SWGTOX) Standard Practices for Method Validation in Forensic Toxicology. *Journal of Analytical Toxicology* **37**, 452-474 (2013). https://doi.org:10.1093/jat/bkt054

9 Liyanage, T. *et al.* Fabrication of a self-assembled and flexible SERS nanosensor for explosive detection at parts-per-quadrillion levels from fingerprints. *Analyst* (2018). https://doi.org:10.1039/C8AN00008E

10 Joshi, G. K., White, S. L., Johnson, M. A., Sardar, R. & Jain, P. K. Ultrashort, Angstrom-Scale Decay of Surface-Enhanced Raman Scattering at Hot Spots. *Journal of Physical Chemistry C* **120**, 24973-24981 (2016). https://doi.org:10.1021/acs.jpcc.6b08242

11 Joshi, G. K. *et al.* Ultrasensitive Photoreversible Molecular Sensors of Azobenzene-Functionalized Plasmonic Nanoantennas. *Nano Letters* **14**, 532-540 (2014). https://doi.org:10.1021/nl403576c

12 Andreou, C., Hoonejani, M. R., Barmi, M. R., Moskovits, M. & Meinhart, C. D. Rapid Detection of Drugs of Abuse in Saliva Using Surface Enhanced Raman Spectroscopy and Microfluidics. *ACS Nano* **7**, 7157-7164 (2013). https://doi.org:10.1021/nn402563f

13 Han, Z. *et al.* Three-Dimensional Surface-Enhanced Raman Scattering Hotspots in Spherical Colloidal Superstructure for Identification and Detection of Drugs in Human Urine. *Anal. Chem.* **87**, 4821-4828 (2015). https://doi.org:10.1021/acs.analchem.5b00176

14 Kline, N. D. *et al.* Optimization of Surface-Enhanced Raman Spectroscopy Conditions for Implementation into a Microfluidic Device for Drug Detection. *Analytical Chemistry (Washington, DC, United States)* **88**, 10513-10522 (2016). https://doi.org:10.1021/acs.analchem.6b02573

15 Ma, Y. *et al.* Surface-Enhanced Raman Spectroscopy on Liquid Interfacial Nanoparticle Arrays for Multiplex Detecting Drugs in Urine. *Analytical Chemistry (Washington, DC, United States)* **88**, 8145-8151 (2016). https://doi.org:10.1021/acs.analchem.6b01884

16 Muehlethaler, C., Leona, M. & Lombardi, J. R. Review of Surface Enhanced Raman Scattering Applications in Forensic Science. *Anal. Chem.* **88**, 152-169 (2016). https://doi.org:10.1021/acs.analchem.5b04131

17 Chen, J. *et al.* Flexible and Adhesive Surface Enhance Raman Scattering Active Tape for Rapid Detection of Pesticide Residues in Fruits and Vegetables. *Analytical Chemistry* **88**, 2149-2155 (2016). https://doi.org:10.1021/acs.analchem.5b03735

18 Peters, F. T. Recent advances of liquid chromatography–(tandem) mass spectrometry in clinical and forensic toxicology. *Clinical Biochemistry* **44**, 54-65 (2011). https://doi.org:https://doi.org/10.1016/j.clinbiochem.2010.08.008

19 Dziadosz, M., Teske, J., Henning, K., Klintschar, M. & Nordmeier, F. LC–MS/MS screening strategy for cannabinoids, opiates, amphetamines, cocaine, benzodiazepines and methadone in human serum, urine and post-mortem blood as an effective alternative to immunoassay based methods applied in forensic toxicology for preliminary examination. *Forensic Chemistry* **7**, 33-37 (2018). https://doi.org:10.1016/j.forc.2017.12.007

20 Xi, W., Shrestha, B. K. & Haes, A. J. Promoting Intra- and Intermolecular Interactions in Surface-Enhanced Raman Scattering. *Analytical Chemistry (Washington, DC, United States)* **90**, 128-143 (2018). https://doi.org:10.1021/acs.analchem.7b04225

21 Liyanage, T. *et al.* Fabrication of a self-assembled and flexible SERS nanosensor for explosive detection at parts-per-quadrillion levels from fingerprints. *Analyst* **143**, 2012-2022 (2018). https://doi.org:10.1039/C8AN00008E

22 Zong, C. *et al.* Surface-Enhanced Raman Spectroscopy for Bioanalysis: Reliability and Challenges. *Chem. Rev.* **118**, 4946-4980 (2018). https://doi.org:10.1021/acs.chemrev.7b00668

23 Joshi, G. K., White, S. L., Johnson, M. A., Sardar, R. & Jain, P. K. Ultrashort, Angstrom-Scale Decay of Surface-Enhanced Raman Scattering at Hot Spots. *J. Phys. Chem. C* **120**, 24973-24981 (2016). https://doi.org:10.1021/acs.jpcc.6b08242

24 Le Ru, E. C., Blackie, E., Meyer, M. & Etchegoin, P. G. Surface Enhanced Raman Scattering Enhancement Factors: A Comprehensive Study. *J. Phys. Chem. C* **111**, 13794-13803 (2007). https://doi.org:10.1021/jp0687908

25 Schlücker, S. Surface-Enhanced Raman Spectroscopy: Concepts and Chemical Applications. *Angew. Chem. Int. Ed.* **53**, 4756-4795 (2014). https://doi.org:10.1002/anie.201205748

26 Moskovits, M. Surface-enhanced Raman spectroscopy: a brief retrospective. *J. Raman Spectrosc.* **36**, 485-496 (2005). https://doi.org:10.1002/jrs.1362

27 Sun, F. *et al.* Hierarchical zwitterionic modification of a SERS substrate enables real-time drug monitoring in blood plasma. *Nat. Commun.* **7**, 13437 (2016). https://doi.org:10.1038/ncomms13437

28 Joshi, G. K., McClory, P. J., Dolai, S. & Sardar, R. Improved localized surface plasmon resonance biosensing sensitivity based on chemically-synthesized gold nanoprisms as plasmonic transducers. *J. Mater. Chem.* **22**, 923-931 (2012).

29 Joshi, G. K. *et al.* Designing Efficient Localized Surface Plasmon Resonance-Based Sensing Platforms: Optimization of Sensor Response by Controlling the Edge Length of Gold Nanoprisms. *J. Phys. Chem. C* **116**, 20990-21000 (2012). https://doi.org:10.1021/jp302674h

30 Liyanage, T., Nagaraju, M., Johnson, M., Muhoberac, B. B. & Sardar, R. Reversible Tuning of the Plasmoelectric Effect in Noble Metal Nanostructures Through Manipulation of Organic Ligand Energy Levels. *Nano Lett.* **20**, 192-200 (2020). https://doi.org:10.1021/acs.nanolett.9b03588

31 Lambert, B. L., Gronert, S., Shurvell, F. H., Lightner, A.,D. Organic Structural Spectroscopy. (2011).

32 Frisch, M. J. T., G. W.; Schlegel, H. B.; Scuseria, G. E.; Robb, M. A.; Cheeseman, J. R.; Scalmani, G.; Barone, V.; Petersson, G. A.; Nakatsuji, H.; Li, X.; Caricato, M.; Marenich, A. V.; Bloino, J.; Janesko, B. G.; Gomperts, R.; Mennucci, B.; Hratchian, H. P.; Ortiz, J. V.; Izmaylov, A. F.; Sonnenberg, J. L.; Williams-Young, D.; Ding, F.; Lipparini, F.; Egidi, F.; Goings, J.; Peng, B.; Petrone, A.; Henderson, T.; Ranasinghe, D.; Zakrzewski, V. G.; Gao, J.; Rega, N.; Zheng, G.; Liang, W.; Hada, M.; Ehara, M.; Toyota, K.; Fukuda, R.; Hasegawa, J.; Ishida, M.; Nakajima, T.; Honda, Y.; Kitao, O.; Nakai, H.; Vreven, T.; Throssell, K.; Montgomery, J. A., Jr.; Peralta, J. E.; Ogliaro, F.; Bearpark, M. J.; Heyd, J. J.; Brothers, E. N.; Kudin, K. N.; Staroverov, V. N.; Keith, T. A.; Kobayashi, R.; Normand, J.; Raghavachari, K.; Rendell, A. P.; Burant, J. C.; Iyengar, S. S.; Tomasi, J.; Cossi, M.; Millam, J. M.; Klene, M.; Adamo, C.; Cammi, R.; Ochterski, J. W.; Martin, R. L.; Morokuma, K.; Farkas, O.; Foresman, J. B.; Fox, D. J. **Gaussian 16, Revision C.01; Gaussian, Inc., Wallingford CT** (2016).

33 Senanayake, R. D., Lingerfelt, D. B., Kuda-Singappulige, G. U., Li, X. & Aikens, C. M. Real-Time TDDFT Investigation of Optical Absorption in Gold Nanowires. *J. Phys. Chem. C* **123**, 14734-14745 (2019). https://doi.org:10.1021/acs.jpcc.9b00296

34 Dennington, R. K., T. A.; Millam, J., M. **GaussView, Version 6; Semichem Inc., Shawnee Mission, KS.** (2016).

35 Haddad, A., Comanescu, M. A., Green, O., Kubic, T. A. & Lombardi, J. R. Detection and Quantitation of Trace Fentanyl in Heroin by Surface-Enhanced Raman Spectroscopy. *Analytical Chemistry (Washington, DC, United States)* **90**, 12678-12685 (2018). https://doi.org:10.1021/acs.analchem.8b02909

36 Halas, N. J., Lal, S., Chang, W.-S., Link, S. & Nordlander, P. Plasmons in Strongly Coupled Metallic Nanostructures. *Chem. Rev.* **111**, 3913-3961 (2011). https://doi.org:10.1021/cr200061k

37 Lee, Y. H. *et al.* Nanoscale surface chemistry directs the tunable assembly of silver octahedra into three two-dimensional plasmonic superlattices. *Nat. Commun.* **6**, 6990-6997 (2015). https://doi.org:10.1038/ncomms7990

38 McFarland, A. D., Young, M. A., Dieringer, J. A. & Van Duyne, R. P. Wavelength-Scanned Surface-Enhanced Raman Excitation Spectroscopy. *J. Phys. Chem. B* **109**, 11279-11285 (2005). https://doi.org:10.1021/jp050508u

39 Liyanage, T. *et al.* Plasmoelectronic-Based Ultrasensitive Assay of Tumor Suppressor microRNAs Directly in Patient Plasma: Design of Highly Specific Early Cancer Diagnostic Technology. *Analytical Chemistry (Washington, DC, United States)* **91**, 1894-1903 (2019). https://doi.org:10.1021/acs.analchem.8b03768

40 Joshi, G. K. *et al.* Highly Specific Plasmonic Biosensors for Ultrasensitive MicroRNA Detection in Plasma from Pancreatic Cancer Patients. *Nano Lett.* **14**, 6955-6963 (2014). https://doi.org:10.1021/nl503220s

41 Zheng, M., Davidson, F. & Huang, X. Ethylene Glycol Monolayer Protected Nanoparticles for Eliminating Nonspecific Binding with Biological Molecules. *J. Am. Chem. Soc.* **125**, 7790-7791 (2003). https://doi.org:10.1021/ja0350278

42 Joshi, G. K., Smith, K. A., Johnson, M. A. & Sardar, R. Temperature-Controlled Reversible Localized Surface Plasmon Resonance Response of Polymer-Functionalized Gold Nanoprisms in the Solid State. *J. Phys. Chem. C* **117**, 26228-26237 (2013). https://doi.org:10.1021/jp409264w

43 Shaikeea, A., Basu, S., Hatte, S. & Bansal, L. Insights into Vapor-Mediated Interactions in a Nanocolloidal Droplet System: Evaporation Dynamics and Affects on Self-Assembly Topologies on Macro- to Microscales. *Langmuir* **32**, 10334-10343 (2016). https://doi.org:10.1021/acs.langmuir.6b03024

44 Li, P. *et al.* Evaporative Self-Assembly of Gold Nanorods into Macroscopic 3D Plasmonic Superlattice Arrays. *Adv. Mater.* **28**, 2511-2517 (2016). https://doi.org:10.1002/adma.201505617

45 Dong, R., Weng, S., Yang, L. & Liu, J. Detection and Direct Readout of Drugs in Human Urine Using Dynamic Surface-Enhanced Raman Spectroscopy and Support Vector Machines. *Analytical Chemistry (Washington, DC, United States)* **87**, 2937-2944 (2015). https://doi.org:10.1021/acs.analchem.5b00137

46 Yang, Y., Lee, J. T., Liyanage, T. & Sardar, R. Flexible Polymer-Assisted Mesoscale Self-Assembly of Colloidal CsPbBr3 Perovskite Nanocrystals into Higher Order Superstructures with Strong Inter-Nanocrystal Electronic Coupling. *J. Am. Chem. Soc.* **141**, 1526-1536 (2019). https://doi.org:10.1021/jacs.8b10083

47 Sardar, R. & Shumaker-Parry, J. S. Asymmetrically Functionalized Gold Nanoparticles Organized in One-Dimensional Chains. *Nano Lett.* **8**, 731-736 (2008). https://doi.org:10.1021/nl073154m

48 Han, Z. *et al.* Portable Kit for Identification and Detection of Drugs in Human Urine Using Surface-Enhanced Raman Spectroscopy. *Anal. Chem.* **87**, 9500-9506 (2015). https://doi.org:10.1021/acs.analchem.5b02899

49 Stiles, P. L., Dieringer, J. A., Shah, N. C. & Van Duyne, R. P. Surface-Enhanced Raman Spectroscopy. *Annu. Rev. Anal. Chem.* **1**, 601-626 (2008). https://doi.org:doi:10.1146/annurev.anchem.1.031207.112814

50 Scarabelli, L., Coronado-Puchau, M., Giner-Casares, J. J., Langer, J. & Liz-Marzán, L. M. Monodisperse Gold Nanotriangles: Size Control, Large-Scale Self-Assembly, and Performance in Surface-Enhanced Raman Scattering. *ACS Nano* **8**, 5833-5842 (2014). https://doi.org:10.1021/nn500727w

51 Vol. DEA Issues Nationwide Alert on Fentanyl as Threat to Health and Public Safety; Drug Enforcement Administration (2018).
52 Lager, P. S., Attema-de Jonge, M. E., Gorzeman, M. P., Kerkvliet, L. E. & Franssen, E. J. F. Clinical value of drugs of abuse point of care testing in an emergency department setting. *Tox. Rep.* **5**, 12-17 (2018). https://doi.org:https://doi.org/10.1016/j.toxrep.2017.12.001
53 Department of Health and Human Services. *Fed. Regist.* **77**, 71858– 71907 (2008).
54 Fedick, P. W., Pu, F., Morato, N. M. & Cooks, R. G. Identification and Confirmation of Fentanyls on Paper using Portable Surface Enhanced Raman Spectroscopy and Paper Spray Ionization Mass Spectrometry. *J. Am. Soc. Mass Spectrom.* **31**, 735-741 (2020). https://doi.org:10.1021/jasms.0c00004
55 Fedick, P. W., Bills, B. J., Manicke, N. E. & Cooks, R. G. Forensic Sampling and Analysis from a Single Substrate: Surface-Enhanced Raman Spectroscopy Followed by Paper Spray Mass Spectrometry. *Analytical Chemistry (Washington, DC, United States)* **89**, 10973-10979 (2017). https://doi.org:10.1021/acs.analchem.7b02798
56 Wang, L., Deriu, C., Wu, W., Mebel, A. M. & McCord, B. Surface-enhanced Raman spectroscopy, Raman, and density functional theoretical analyses of fentanyl and six analogs. *J. Raman Spectrosc.* **50**, 1405-1415 (2019). https://doi.org:10.1002/jrs.5656
57 Templeton, A. C., Wuelfing, W. P. & Murray, R. W. Monolayer-Protected Cluster Molecules. *Acc. Chem. Res.* **33**, 27-36 (2000). https://doi.org:10.1021/ar9602664
58 Langer, J. *et al.* Present and Future of Surface-Enhanced Raman Scattering. *ACS Nano* **14**, 28-117 (2020). https://doi.org:10.1021/acsnano.9b04224
59 Masterson, A. N. *et al.* A novel liquid biopsy-based approach for highly specific cancer diagnostics: mitigating false responses in assaying patient plasma-derived circulating microRNAs through combined SERS and plasmon-enhanced fluorescence analyses. *Analyst* **145**, 4173-4180 (2020). https://doi.org:10.1039/D0AN00538J
60 Smith, J. P., Sutcliffe, O. B. & Banks, C. E. An overview of recent developments in the analytical detection of new psychoactive substances (NPSs). *Analyst* **140**, 4932-4948 (2015). https://doi.org:10.1039/C5AN00797F
61 Stuart, D. A., Biggs, K. B. & Van Duyne, R. P. Surface-enhanced Raman spectroscopy of half-mustard agent. *Analyst* **131**, 568-572 (2006). https://doi.org:10.1039/B513326B
62 Yu, W. W. & White, I. M. Inkjet-printed paper-based SERS dipsticks and swabs for trace chemical detection. *Analyst* **138**, 1020-1025 (2013). https://doi.org:10.1039/c2an36116g
63 Sardar, R., Park, J.-W. & Shumaker-Parry, J. S. Polymer-Induced Synthesis of Stable Gold and Silver Nanoparticles and Subsequent Ligand Exchange in Water. *Langmuir* **23**, 11883-11889 (2007). https://doi.org:10.1021/la702359g
64 Hao, E. & Schatz, G. C. Electromagnetic fields around silver nanoparticles and dimers. *J. Chem. Phys.* **120**, 357-366 (2004).
65 Joshi, G. K. *et al.* Label-Free Nanoplasmonic-Based Short Noncoding RNA Sensing at Attomolar Concentrations Allows for Quantitative and Highly Specific Assay of MicroRNA-10b in Biological Fluids and Circulating Exosomes. *ACS Nano* **9**, 11075-11089 (2015). https://doi.org:10.1021/acsnano.5b04527
66 Burr, D. S. *et al.* Integrating SERS and PSI-MS with Dual Purpose Plasmonic Paper Substrates for On-Site Illicit Drug Confirmation. *Analytical Chemistry (Washington, DC, United States)* **92**, 6676-6683 (2020). https://doi.org:10.1021/acs.analchem.0c00562

67 Liyanage, T. *et al.* Optimization of electromagnetic hot spots in surface-enhanced Raman scattering substrates for an ultrasensitive drug assay of emergency department patients' plasma. *Analyst* **145**, 7662-7672 (2020). https://doi.org:10.1039/D0AN01372B

68 Park, S., Lee, J. & Ko, H. Transparent and Flexible Surface-Enhanced Raman Scattering (SERS) Sensors Based on Gold Nanostar Arrays Embedded in Silicon Rubber Film. *ACS Appl. Mater. Interfaces* **9**, 44088-44095 (2017). https://doi.org:10.1021/acsami.7b14022

69 Deriu, C., Conticello, I., Mebel, A. M. & McCord, B. Micro Solid Phase Extraction Surface-Enhanced Raman Spectroscopy (μ-SPE/SERS) Screening Test for the Detection of the Synthetic Cannabinoid JWH-018 in Oral Fluid. *Analytical Chemistry (Washington, DC, United States)* **91**, 4780-4789 (2019). https://doi.org:10.1021/acs.analchem.9b00335

70 Izquierdo-Lorenzo, I., Sanchez-Cortes, S. & Garcia-Ramos, J. V. Adsorption of Beta-Adrenergic Agonists Used in Sport Doping on Metal Nanoparticles: A Detection Study Based on Surface-Enhanced Raman Scattering. *Langmuir* **26**, 14663-14670 (2010). https://doi.org:10.1021/la102590f

71 . *https://www.cdc.gov/drugoverdose/index.html, Accessed Sept, 2020.* (2020).

72 Bills, B. J. & Manicke, N. E. Development of a prototype blood fractionation cartridge for plasma analysis by paper spray mass spectrometry. *Clinical Mass Spectrometry* **2**, 18-24 (2016). https://doi.org:https://doi.org/10.1016/j.clinms.2016.12.002

73 McKenna, J., Jett, R., Shanks, K. & Manicke, N. E. Toxicological Drug Screening using Paper Spray High-Resolution Tandem Mass Spectrometry (HR-MS/MS). *Journal of Analytical Toxicology* **42**, 300-310 (2018). https://doi.org:10.1093/jat/bky001

74 Gong, Z. *et al.* Fabrication of SERS Swab for Direct Detection of Trace Explosives in Fingerprints. *ACS Appl. Mater. Interfaces* **6**, 21931-21937 (2014). https://doi.org:10.1021/am507424v

75 Haddad, A., Comanescu, M. A., Green, O., Kubic, T. A. & Lombardi, J. R. Detection and Quantitation of Trace Fentanyl in Heroin by Surface-Enhanced Raman Spectroscopy. *Analytical Chemistry (Washington, DC, United States)* **90**, 12678-12685 (2018). https://doi.org:10.1021/acs.analchem.8b02909

76 Yang, N., You, T.-T., Gao, Y.-K., Zhang, C.-M. & Yin, P.-G. Fabrication of a Flexible Gold Nanorod Polymer Metafilm via a Phase Transfer Method as a SERS Substrate for Detecting Food Contaminants. *Journal of Agricultural and Food Chemistry* **66**, 6889-6896 (2018). https://doi.org:10.1021/acs.jafc.8b01702

77 Zhong, L.-B. *et al.* Self-Assembly of Au Nanoparticles on PMMA Template as Flexible, Transparent, and Highly Active SERS Substrates. *Anal. Chem. (Washington, DC, U. S.)* **86**, 6262-6267 (2014). https://doi.org:10.1021/ac404224f

78 Kang, H., Heo, C.-J., Jeon, H. C., Lee, S. Y. & Yang, S.-M. Durable Plasmonic Cap Arrays on Flexible Substrate with Real-Time Optical Tunability for High-Fidelity SERS Devices. *ACS Appl. Mater. Interfaces* **5**, 4569-4574 (2013). https://doi.org:10.1021/am400019v

79 Lu, G., Li, H. & Zhang, H. Nanoparticle-coated PDMS elastomers for enhancement of Raman scattering. *Chemical Communications (Cambridge, United Kingdom)* **47**, 8560-8562 (2011). https://doi.org:10.1039/c1cc12027a

80 Park, S., Lee, J. & Ko, H. Transparent and Flexible Surface-Enhanced Raman Scattering (SERS) Sensors Based on Gold Nanostar Arrays Embedded in Silicone Rubber Film. *ACS Appl. Mater. Interfaces* **9**, 44088-44095 (2017). https://doi.org:10.1021/acsami.7b14022

81 Wang, X. *et al.* Sensitive Surface-Enhanced Raman Scattering Detection Using On-Demand Postassembled Particle-on-Film Structure. *ACS Appl. Mater. Interfaces* **9**, 31102-31110 (2017). https://doi.org:10.1021/acsami.7b08818

82 Liu, X., Wang, J., Wang, J., Tang, L. & Ying, Y. Flexible and Transparent Surface-Enhanced Raman Scattering (SERS)-Active Metafilm for Visualizing Trace Molecules via Raman Spectral Mapping. *Anal. Chem. (Washington, DC, U. S.)* **88**, 6166-6173 (2016). https://doi.org:10.1021/acs.analchem.6b00858

83 Chen, J. *et al.* Flexible and Adhesive Surface Enhance Raman Scattering Active Tape for Rapid Detection of Pesticide Residues in Fruits and Vegetables. *Analytical Chemistry (Washington, DC, United States)* **88**, 2149-2155 (2016). https://doi.org:10.1021/acs.analchem.5b03735